AMERICAN UNIVERSITY OF BEIRUT

OPTIMIZED DESIGN AND OPERATION OF HEAT-PIPE PV/T SYSTEM WITH PHASE CHANGE MATERIAL FOR THERMAL STORAGE

by
ABED EL HASSAN ALI SWEIDAN

A thesis
submitted in partial fulfillment of the requirements
for the degree of Master of Mechanical Engineering
to the Department of Mechanical Engineering
of the Faculty of Engineering and Architecture
at the American University of Beirut

Beirut, Lebanon
August 2015

AMERICAN UNIVERSITY OF BEIRUT

OPTIMIZED DESIGN AND OPERATION OF HEAT-PIPE PV/T SYSTEM WITH PHASE CHANGE MATERIAL FOR THERMAL STORAGE

by

ABED EL HASSAN ALI SWEIDAN

Approved by:

August 27, 2015

Prof. Nesreen Ghaddar PhD, Professor
Department of Mechanical Engineering — Advisor

August 27, 2015

Prof. Kamel Abou Ghali, PhD, Professor
Department of Mechanical Engineering — Co-Advisor

August 27, 2015

Prof. Sami Karaki PhD, Professor
Department of Electrical and Computer Engineering — Member of Committee

Date of thesis defense: August 25, 2015

AMERICAN UNIVERSITY OF BEIRUT

THESIS, DISSERTATION, PROJECT RELEASE FORM

Student Name: Sweidan Abed El Hassan Ali
Last First Middle

☒ Master's Thesis ○ Master's Project ○ Doctoral Dissertation

☒ I authorize the American University of Beirut to: (a) reproduce hard or electronic copies of my thesis, dissertation, or project; (b) include such copies in the archives and digital repositories of the University; and (c) make freely available such copies to third parties for research or educational purposes.

☐ I authorize the American University of Beirut, **three years after the date of submitting my thesis, dissertation, or project,** to: (a) reproduce hard or electronic copies of it; (b) include such copies in the archives and digital repositories of the University; and (c) make freely available such copies to third parties for research or educational purposes.

Signature 27/08/2015
Date

ACKNOWLEDGMENTS

I would like to express my deepest gratitude for Dr. Nesreene Ghaddar for her advisory, guidance and patience through my graduate study.

I would also like to thank Dr. Kamel Abou Ghali for his recommendations, thoughtful ideas and help in completing this work.

Special thanks to Dr. Sami Karaki for being a member of my thesis committee.

I would also like to show deep gratitude to my family members and friends for their support throughout the past years.

AN ABSTRACT OF THE THESIS OF

Abed El Hassan Ali Sweidan for Master of Engineering
Major: Mechanical Engineering

Title: Optimized Design and Operation of Heat-Pipe PV/T System with Phase Change Material for Thermal Storage

This work aims to study performance of a heat pipe photovoltaic-thermal (HP-PV/T) panel integrated with phase change material (PCM) thermal storage water tank to produce electricity and hot water for an office building. A transient mathematical model for the HP-PV/T was developed to predict its performance at given PCM melting point. The model predicted the PV panel temperature, electrical power output and hot water temperature. The model was validated experimentally using PCM at 29°C melting-point in Beirut climate during the month of July.

The validated model was applied on a typical office space in the city of Beirut to obtain optimal design using a derivative free genetic algorithm. The incremental system cost associated with heat pipe and PCM tank was used in the optimization to obtain the design resulting in minimum annual auxiliary heating cost to meet hot water demand while providing the electricity needs at lower number of PV panels due to improved PV efficiency. An optimal system of 4 kW (20 PV panels each at 1.6 m^2) was found to meet the electric power needs all year round. The optimal PCM storage tank size per panel was 37 liter at PCM total mass of 22.42 kg with melting temperature of 33°C.

CONTENTS

NOMENCLATURE

A	area, m^2
C	specific heat capacity J/kg·K
D	diameter, m
E	output electricity, W/m^2
G	solar radiation intensity W/m^2
h	heat-transfer coefficient, $W/m^2 \cdot K$
k	thermal conductivity, W/m·K
L	length, m
M	mass, kg
m	Mesh number
n	number
R	thermal resistance K/W
T	temperature, ^oC
t	time, s
u	Flow velocity, m/s
Pr	Prandtl number
Nu	Nusselt number
Ra	Raleigh number
Gr	Grashof number
x	lateral direction of heat pipe fin plate
X	PCM liquid fraction

Greek Symbols

α	absorptivity, thermal diffusivity, m^2/s
γ	PV cells coverage ratio
δ	thickness, m
ε	emissivity
ξ	porosity

η	efficiency
θ	angle, (°)
ρ	density, kg/m^3, reflectance
τ	transmittance
β	volumetric thermal expansion, K^{-1}
μ	dynamic viscosity, Pa·s
v	kinematic viscosity, m^2/s

Subscripts

a	air, ambient
b	base panels
ad	adhesive layer
i	Inner, differential node
l	liquid
o	outer
p	heat pipe
s	thermal insulating material
v	vapor
w	water, wall of the heat pipe
cond	condenser section of the heat pipe
evap	evaporator section of the heat pipe
sky	sky
wick	wick of the heat pipe

ILLUSTRATIONS

TABLES

CHAPTER I

INTRODUCTION

Renewable energy is being widely used in many countries as a practical alternative to fossil fuels and a solution for serious environmental problems. Solar energy has a very big potential compared to other forms of renewable energy. The Earth receives energy from sunlight in one hour $\left(4.3\times10^{20}J\right)$ that is enough to cover the worldwide energy consumption needs throughout one year $\left(4.1\times10^{20}J\right)$ [1]. The most spread way of making use of solar energy is by the use of Photovoltaics where sunlight is directly converted into electrical current that can be utilized to power electrical appliances. This technology was invented by Charles Fritts in 1894 and was referred to as the PV cell [2]. However, during the operation of the PV cell, only around 15% of solar radiation is converted to electricity and the rest is converted to heat [3]. The electrical power generation of the PV cell depends greatly on its operating temperature. PV panels' efficiencies are at best 19%, and in most cases in the vicinity of 10%, rarely reaching 15% for commercially available panels [4]. The PV cell's efficiency drops with the increase in the operating temperature: an increase of 30 degrees K in cell's temperature can cause a drop of 15% in the electrical efficiency [5]. Therefore, reducing the operating temperature of photovoltaic cell is important to boost its electrical efficiency. Cooling the PV panels became an interesting topic for researchers, and many studies have been carried out to counter the temperature effect on PV cells. Various active and passive cooling methods have been researched and analyzed to date. When

cooling the PV panels and using the extracted thermal energy for low temperature applications, e.g. water and air heating, the system is referred to as hybrid photovoltaic/thermal (PV/T) system that produces both electricity and heat from one integrated component or system [6].

Photovoltaic thermal (PV/T) panels have a higher energy yield per unit area than separate systems of PV panels and solar collectors [7]. PV/T offers the advantage of providing both high-grade electrical energy and low-grade thermal energy [8-9]. The increased electrical energy due to cell cooling makes the PV/T an attractive alternative to conventional electricity and makes the panels more cost competitive since increased energy yield means a shorter payback period and lower PV area [10].

Different techniques are implemented for cooling the PV panels using air or water as a coolant to maintain lower operating temperatures [3-15]. Air PV/T cooling, despite improved performance with the use of fins, had relatively poor heat removal effectiveness due to the low thermal capacity and conductivity of air [3-5]. Water PV/T cooling is found to be more efficient than PV/T Air systems due to higher water capacity and higher heat transfer coefficients between water and PV back metal cover [6-7]. The PV/T system output was shown in the experimental study of Odeh and Behnia [6] to increase by 4–10%. The average PV/T system's annual electrical efficiency was reported by Kalogirou [7] to increase from 2.8% to 7.7% at payback period of 4.6 years. Krauter [8] used a flowing water film above the PV modules and reported a decrease up to 22°C in surface temperature with a net-electrical gain of 8–9%. Although active cooling of the PV panels by water is effective. It requires additional power consumption that reduces the net gain of the efficiency.

Regardless of air or water selection as the cooling medium, it should be noted that the temperature of solar PV panel increases along the fluid flowing direction, leading to non-uniform cooling which hampers the control of panel temperature for enhancement of the photoelectric conversion efficiency [11]. Gang et al. [12] introduced a heat pipe PV/T panels to improve cooling non-uniformity at the back of the panel utilizing high latent heat transfer rates that are associated with extremely small temperature drops between the heated and the cooled region and hence enhance the photoelectric conversion performance [11-12-13]. Ghaddar and Nasr [16] conducted an experimental study on integrated heat-pipe, solar collector, and storage tank and showed that the system efficiency dropped when storage tank temperature increased due to build-up of stored energy in the condenser side. Mathioulakis and Belessiotis [13] reported similar performance of a wickless gravity assisted loop heat-pipe for the heat transfer from the collector–evaporator to the tank–condenser. The energy behavior of their system was characterized by high, instantaneous efficiencies up to 60%, wide temperature operating range and effective operation with small temperature differences between the collector and tank [13]. However, the temperature increase in the tank caused an increase in temperature for the whole heat-pipe, thus increasing the losses from the collector which resulted in a decrease of the overall system efficiency.

Given that the solar energy source is often intermittent and time-dependent; the performance of the heat pipe PV/T cannot be sustained unless the sink temperature (storage tank) can be controlled. The integration of a PV/T collector with a hot water storage tank was found to be an economically feasible idea. However, increasing the hot water temperature in order to meet some application requirements would in turn cause a reduction in the power generation efficiency of solar PV [17]. In addition, water has a

low energy density resulting in a bulky storage system. Latent heat storage systems using phase change materials (PCMs) are particularly more attractive than sensible heat storage systems due to their high energy storage capacity and their ability to store heat at a constant temperature [18]. Abhat [18] reviewed the different PCMs used for low temperature latent heat storage in the range 0-120°C and investigated their melting and freezing behavior. Sharma et al. [19] investigated and analyzed the available thermal energy storage systems incorporating PCMs for use in different applications including solar water-heating systems. Prakash et al. [20] analyzed the performance of a novel built-in storage type water heater containing a layer of PCM-filled capsules and reported a more efficient and more suitable storage system during off-sunshine hours when compared with a system having no PCM storage. Cabeza et al. [21, 22] reported that the inclusion of a PCM module in hot water storage tanks is a very promising technology that provides hot-water for longer periods at smaller tank size.

The objective of this study work is to develop transient mathematical models for the HP-PV/T to predict the integrated system performance in producing electricity and hot water for given environmental and solar conditions, refrigerant-based HP evaporator temperature and PCM melting point. Heat pipes are used to cool the PV panel and dissipate heat into a PCM-water storage tank. The system will take the advantage of adding PCM as a latent storage medium in the heat sink side in order to control the sink temperature, provide efficient thermal energy storage and PV panel cooling. The developed integrated model will be experimentally validated using an experimental setup for the HP-PV/T system. The mathematical model of Gang et al. [12] for the PV panel cooling with heat pipes is adopted in this work, with some modifications to meet our current design. Gang et al. [12] used the forced convection

heat transfer in the PV/T panel heat sink through utilizing cooling water flowing over the condensers, however in our case the heat sink contained stationary water with PCM spheres and the heat transfer is represented by natural convection between the different components. Moreover, Gang et al. utilized sensible heat storage through using a big water storage tank, however in our case the thermal storage was mainly in the latent form through including PCM in the heat sink. This allowed us to eliminate the need for a bulky water storage medium.

The HP-PV/T-PCM system simulation model is applied to a case study of a typical office in Beirut to obtain an optimal design that minimizes the auxiliary heating energy for domestic hot water while meeting the basic electric needs throughout the year at lowest number of PV/T panels and PCM mass. Once optimal design is achieved, the life cycle cost of the system will be determined as well as the payback period for incremental cost of PV cooling system.

CHAPTER II

HP-PV/T-PCM SYSTEM DESCRIPTION

The proposed heat pipe HP-PV/T-PCM system is composed of a PV panel with its metal base joined to the sealed heat pipe tubes evaporator section by a thin, high thermally conductive and adhesive aluminum layer while the condenser section of the heat pipe is immersed in water-PCM storage tank. Figure 1 shows the installed heat pipes at the back of the PV panel and Figure 2 illustrates a side view of the proposed system.

The heat pipe is a sealed metal tube with an inner lining of wick like capillary material and a small amount of fluid in a partial vacuum. It transfers the heat from the PV panel by the process of evaporation in the HP evaporator, vapor flow, condensation in the condenser (water-PCM tank), and then condensate return to the evaporator section by gravity and capillary forces in the distributed wick. Figure 3 shows the operation of the heat pipe. The wick is a thin steel wire mesh placed along the inner diameter of the heat pipe and creates a porous medium with a definite porosity, permeability, thermal conductivity and heat transfer coefficient. The wick structure is included in the current design pipe to improve contact between the heat pipe wall and the liquid and to ensure the even distribution of the liquid on the evaporator surface. Since the heat pipe is operating in gravity-assisted mode, no wick is required in the condenser because gravity drains the condensate from the wall to the paddle. The heat released from the heat pipe condensing end is then transferred through the water to the PCM spheres placed inside the storage tank.

The PCM spheres are made of a latent heat storage material placed inside highly conductive spherical capsules. The tank heat storage capacity is greatly enhanced with the presence of the PCMs. The temperature of the PCMs rises as they absorb heat, and once their temperature reaches the melting point, the PCM starts melting and absorbs large amounts of heat without change in temperature. When the temperature in the surrounding water drops, the PCM solidifies releasing its stored latent heat to the water. Thus the presence of PCMs reduces the temperature fluctuations in the storage tank despite transient incident solar radiation. Figure 4 shows the PCM placed inside the storage tank.

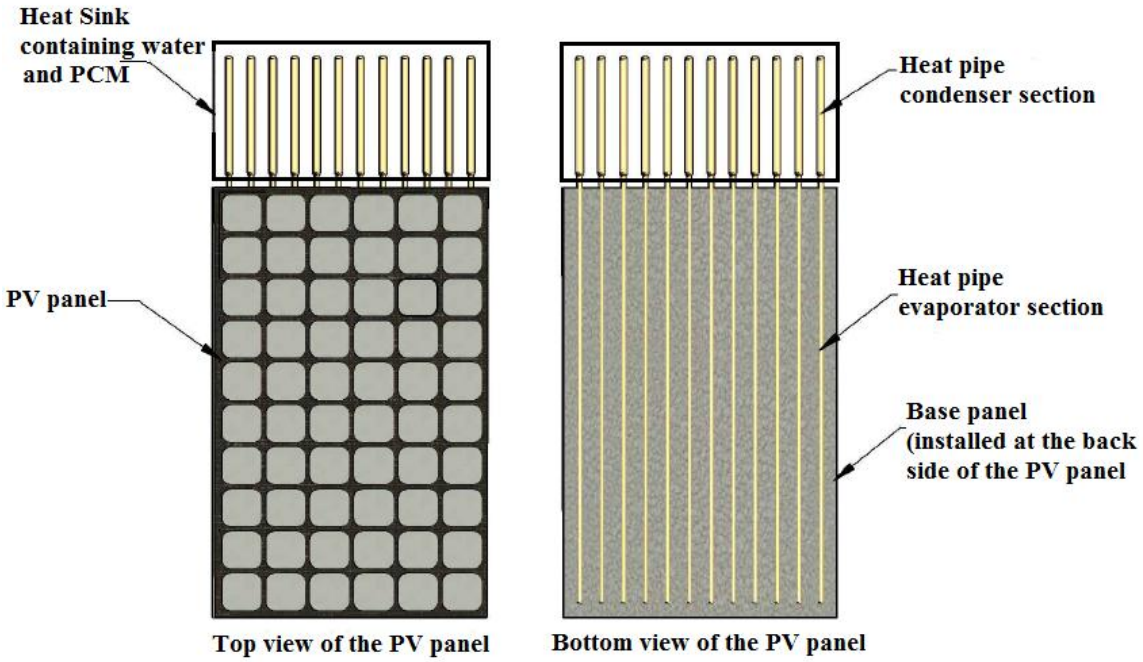

Figure 1: Schematic showing the installed heat pipes at the back side of the PV panel

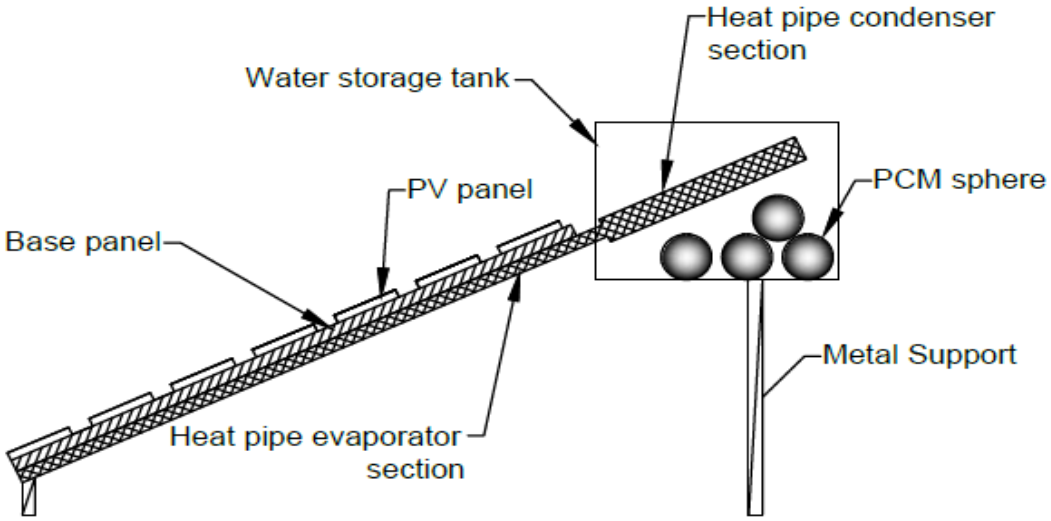

Figure 2: Side view of the proposed system

Transient mathematical models for the different subsystems of the HP-PV/T-PCM system are developed; the PV panel, base panel, and the refrigerant-based heat pipe model using Gang et al. formulation [12], and water-PCM storage tank model. The integrated HP-PV/T-PCM model and its predictions of electrical and thermal outputs will be validated experimentally in Beirut climate. The system model is then applied to a case study and optimization is performed to find the minimum number of PV/T Panels and PCM quantity for a typical office application in Beirut City, in order to minimize the auxiliary energy needed for heating domestic water while meeting the electrical needs on a yearly balanced basis over the whole lifecycle of the system. The electricity is sold and bought at the same price and any excess yearly electricity will have zero value.

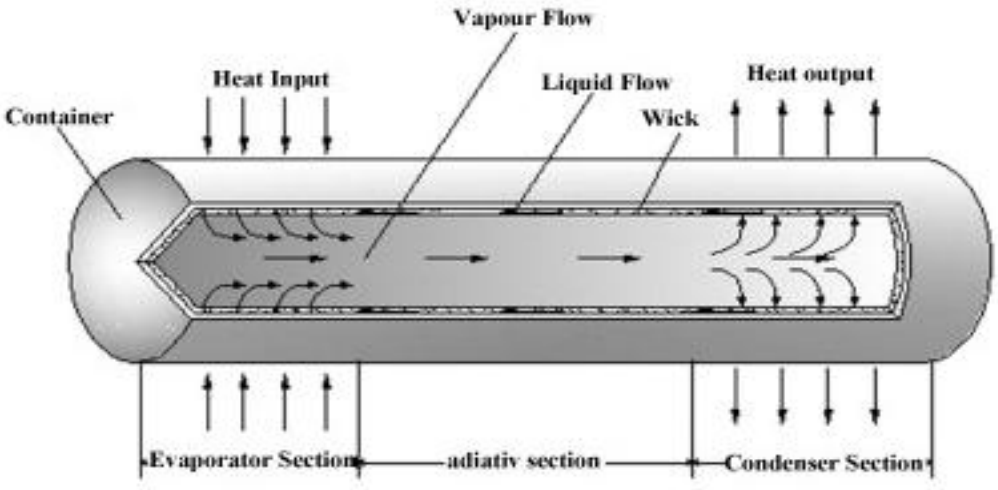

Figure 3: Operation of the heat pipe [14]

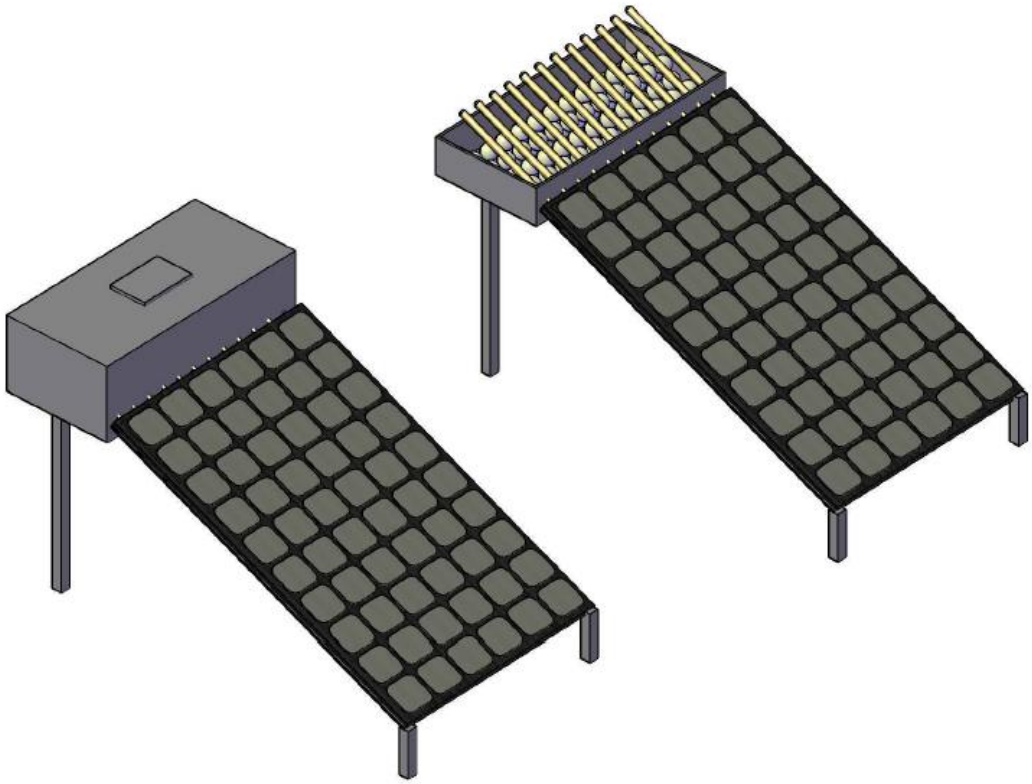

Figure 4: 3D view of the PV system with a tank section showing the PCM spheres

CHAPTER III

MATHEMATICAL MODELLING AND EXPERIMENTAL VALIDATION

A. Mathematical Modelling

In order to write the energy balance equation for each component of the PV/T system, quasi-steady state operation is assumed and the heat pipe is treated as finned plate with heat pipe evaporator section representing the fin base temperature (fluid evaporation temperature) while taking into consideration thermal wall and contact resistances of the pipe [23]. The main energy balance equations include: heat-balance equation of the PV panel, heat conduction along the base panel, heat-balances of the heat pipe, and heat balance for the water-PCM storage tank. The following assumptions have been made in the model as described in [11] and [12]:

- The temperature variation along the thickness of the PV panel and base panel is negligible, because their thickness is much less than their width.
- The temperature variation of the PV panel and base panel along the axial direction of heat pipe is negligible, because of the uniformity of heat pipe operating temperature.

The numerical model of Gang et al. [12] for glazed PV panel with heat pipe is adapted in this work. The PV heat balance equation is given by

$$\delta_{pv}\,\rho_{pv}\,C_{pv}\,\frac{\partial T_{pv}}{\partial t} = h_a\,(T_a - T_{pv}) + h_{sky,pv}\,(T_{sky} - T_{pv}) + \frac{(T_b - T_{pv})}{R_{b,pv}} + \alpha_{pv}\,G - E_{pv} \quad \text{(1a)}$$

The parameters δ_{pv}, ρ_{pv} and α_{pv} are the thickness, density, and absorptivity of the PV panel, respectively, while h_a and $h_{sky,pv}$ are convective and radiant heat-transfer coefficients, between the PV panel and surroundings. The temperatures T_{pv} and T_b are the temperatures of the PV panel and base panel, respectively, and T_{sky} is the sky temperature, $T_{sky} = 0.0552\, T_a^{1.5}$ [23]. The convective and radiant heat-transfer coefficients between the PV-panel and surroundings are given, respectively, as [23]:

$$h_a = 2.8 + 3u_a$$

$$h_{sky,pv} = \varepsilon_{pv}\,\sigma(T_{sky}^2 + T_{pv}^2)(T_{sky} + T_{pv})$$

where, u_a is the wind speed, ε_{pv} is the emissivity of the PV panel and σ is the Stefan–Boltzmann constant $\sigma = 5.670373\times10^{-8}\, W\, m^{-2}\, K^{-4}$.

The parameter $R_{b,pv}$ is the thermal contact resistance of the adhesive material between the PV layer and metal base panel, $R_{b,pv} = \dfrac{\delta_{ad}}{k_{ad}}$

where, δ_{ad} and k_{ad} are the thickness and thermal conductivity of the adhesive material that connects the PV module to the base panel. The electrical energy produced by the PV panel E_{pv} is given by [12]:

$$E_{pv} = \gamma\, \alpha_{\mathrm{pv}} G \eta_r \left[\, 1 - Br(T_{pv} - T_r)\right] \qquad (1b)$$

where G is the solar irradiation, γ is the PV cell coverage ratio $\gamma = A_{pv} / A_c$, η_r is the reference cell efficiency at the reference operating temperature $T_r = 298.15\ K$, and temperature coefficient is $B_r = 0.0045\ K^{-1}$. The electrical efficiency of the system is given by

$$\eta_{electrical} = \frac{E_{pv}}{G} \tag{1c}$$

Gang et al. [12] divided the base panel into differential grids where one grid is connected to a heat pipe (heat-pipe node) and the other is in the middle of connecting panel (fin plate) as shown in Fig. 5. The 1-D heat-conduction equations for these nodes were derived in their work [12] neglect the temperature variation of the base panel along the axial direction of the heat pipe because of the uniformity of the heat pipe temperature and are given by

For the middle node:

$$\rho_b C_b \frac{\partial T_b}{\partial t} = k_b \frac{\partial^2 T_b}{\partial x^2} + \frac{1}{\delta_b}\left(\frac{(T_a - T_b)}{R_{b,a}} + \frac{(T_{pv} - T_b)}{R_{b,pv}}\right) \tag{2}$$

For the heat pipe node:

$$\rho_b C_b \frac{\partial T_b}{\partial t} = k_b \frac{\partial^2 T_b}{\partial x^2} + \frac{1}{\delta_b}\left(\frac{(T_a - T_b)}{R_{b,a}} + \frac{(T_{pv} - T_b)}{R_{b,pv}} + \frac{(T_{p,evap} - T_b)}{R_{p,b}}\right) \tag{3}$$

The parameters δ_b, ρ_b, and C_b are the base panel thickness, density and specific heat, respectively. T_b , T_{pv} and $T_{p,evap}$ are the base panel, PV panel and evaporator section temperatures respectively. The base panel temperature (T_b) is considered to be uniform along the axial direction of heat pipe, because of the uniformity of heat pipe operating temperature. $R_{b,a}$ is the thermal resistance between the base panel and the ambient air, given by:

$$R_{b,a} = \frac{\delta_s}{k_s} + \frac{1}{h_a}$$

Where, δ_s and k_s are the thickness and the thermal conductivity of the insulation material, respectively as indicated in Figure 5.

and $R_{b,p}$ is the thermal resistance between the base panel and the inner wall of heat pipe evaporator section [12].

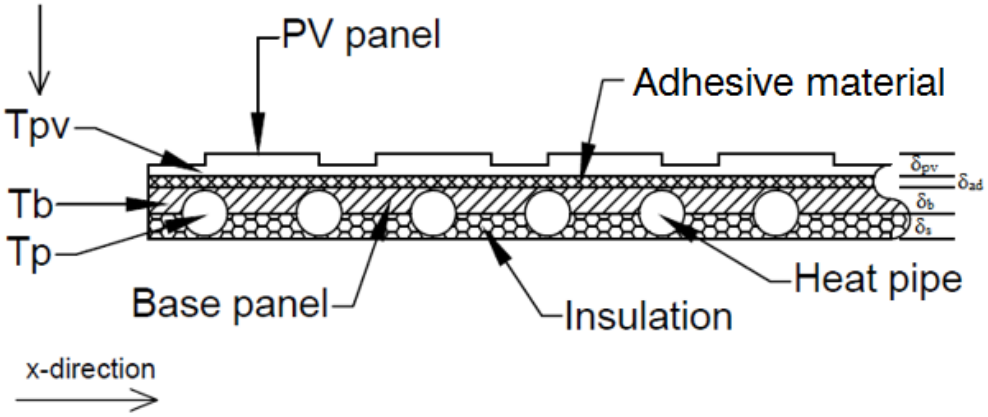

Figure 5: Section of the HP-PV/T solar collector

The heat pipe evaporator section assumes that evaporation of the refrigerant takes place at a constant saturation pressure since the pressure drop caused by vapor flow along the axial length of the heat pipe is very small and can be neglected in accordance with the models of Ghaddar and Nasr [16] and Gang et al. [12] developed for the energy transport in the heat pipe. The heat balance equations for the evaporator and condenser sections are given by

Evaporator: $$M_{p,evap}C_p\frac{\partial T_{p,evap}}{\partial t}=\frac{T_{p,cond}-T_{p,evap}}{R_{evap,cond}}+\frac{T_b-T_{p,evap}}{R_{p,b}} \quad (4)$$

Condenser: $$M_{p,cond}C_p\frac{\partial T_{p,cond}}{\partial t}=\frac{T_{p,evap}-T_{p,cond}}{R_{evap,cond}}+A_{cond,w}h_{cond,w}\left(T_w-T_{p,cond}\right) \quad (5)$$

where $T_{p,cond}$ and $T_{p,evap}$ are the temperatures of the condenser and evaporator sections of the heat pipe, respectively. $M_{p,evap}$ and $M_{p,cond}$ are the masses of the evaporator and condenser sections of the heat pipe, respectively. $R_{evap,cond}$ is the total thermal resistance of heat transfer from the evaporator section to the condenser section which takes into consideration the wick resistance (as described in Ref. [12]). $A_{cond,w}$ is the contact area between the condenser section of the heat pipe and the water in the storage tank. The convection heat-transfer coefficients between the heat-pipe condenser section and water in the storage tank is $h_{cond,w}$ [24].

The heat transfer from the evaporator section to the condenser section of the heat pipe may be mathematically modelled by using the total thermal resistance $R_{evap,cond}$ (Fig. 6). The value of $R_{evap,cond}$ can be derived based on the following:

$$R_{evap,cond} = R_{evap,wick} + R_{evap,i} + R_{v} + R_{cond,i}$$

Within the evaporator section, the thermal resistances which account for temperature drops are the wick conduction resistance and internal resistance at the vapour-liquid interface. In the vapour space, the pressure drops are very small, and the vapour space is assumed to operate at constant saturation pressure and temperature along the axial length of the heat pipe. Therefore, the thermal resistance in the vapour flow direction (R_v) can be neglected as described in [11, 12].

$R_{evap,wick}$ is the thermal resistances across the wick thickness, and may presented as follows

$$R_{evap,wick} = \frac{ln\left(D_{wick,o}/D_{wick,i}\right)}{2\pi L_{evap} k_{wick}}$$

where, k_{wick} is the effective thermal conductivity of the saturated wick screen mesh structure used in the evaporator section and can be calculated as:

$$k_{wick} = \frac{k_l \left[(k_l + k_s) - (1 - \xi_{wick})(k_l - k_s) \right]}{(k_l + k_s) + (1 - \xi_{wick})(k_l - k_s)}$$

k_l : Thermal conductivity of the working fluid

k_s : Thermal conductivity of the wick material

ξ_{wick} : Porosity of the wick

The thermal resistance occurring at the vapor-liquid interfaces in the evaporator can be calculated by (Azad [25])

$$R_{evap,i} = \frac{2}{\pi D_{evap,i} L_{evap} h_{evap,i}}$$

where $h_{evap,i}$ is the film coefficient and is equal to the thermal conductivity of the working fluid divided by the wick thickness (t_{wick}) given by:

$$h_{evap,i} = \frac{k_l}{t_{wick}}$$

The vapour condenses on the inner wall of the condenser while releasing the latent heat of condensation. The thermal resistance associated with the condensing process is defined as:

$$R_{cond,i} = \frac{1}{\pi D_{cond,i} L_{cond} h_{cond,i}}$$

where $h_{cond,i}$ is the condensing film coefficient and is given by [26]:

$$h_{cond,i} = 1.13\left[\frac{g\sin\theta.\rho_l(\rho_l-\rho_v)k_l^3 h_{fg}}{\mu_l \Delta T_{cr} L_{cond}}\right]^{\frac{1}{4}}$$

ρ_l and ρ_v are the liquid and vapour densities of the working fluid inside the heat pipe respectively. The critical temperature difference of the condenser is given by:

$\Delta T_{cr} = \left|T_{cond,i} - T_l\right|$ where, $T_{cond,i}$ and T_l are the condenser surface temperature and the working fluid saturation temperature respectively.

The working fluid saturated temperature (T_l) is calculated according to Hussein et al. [27] assuming that the working fluid inside the heat pipe is a wholly saturated liquid, because the density of the working fluid vapor phase is so small compared to its liquid phase density.

$$\frac{\pi}{4} D_{evap,i}^2 L_{evap} \rho_l C_l V^* \frac{\partial T_l}{dt} = \pi D_{evap,i} L_{evap} h_{evap,i}\left(T_{p,evap} - T_l\right) - \pi D_{cond,i} L_{cond} h_{cond,i}\left(T_l - T_{p,cond}\right) \quad (6)$$

where V^* is the liquid filling ratio (volume liquid / volume of the evaporator section of the heat pipe)

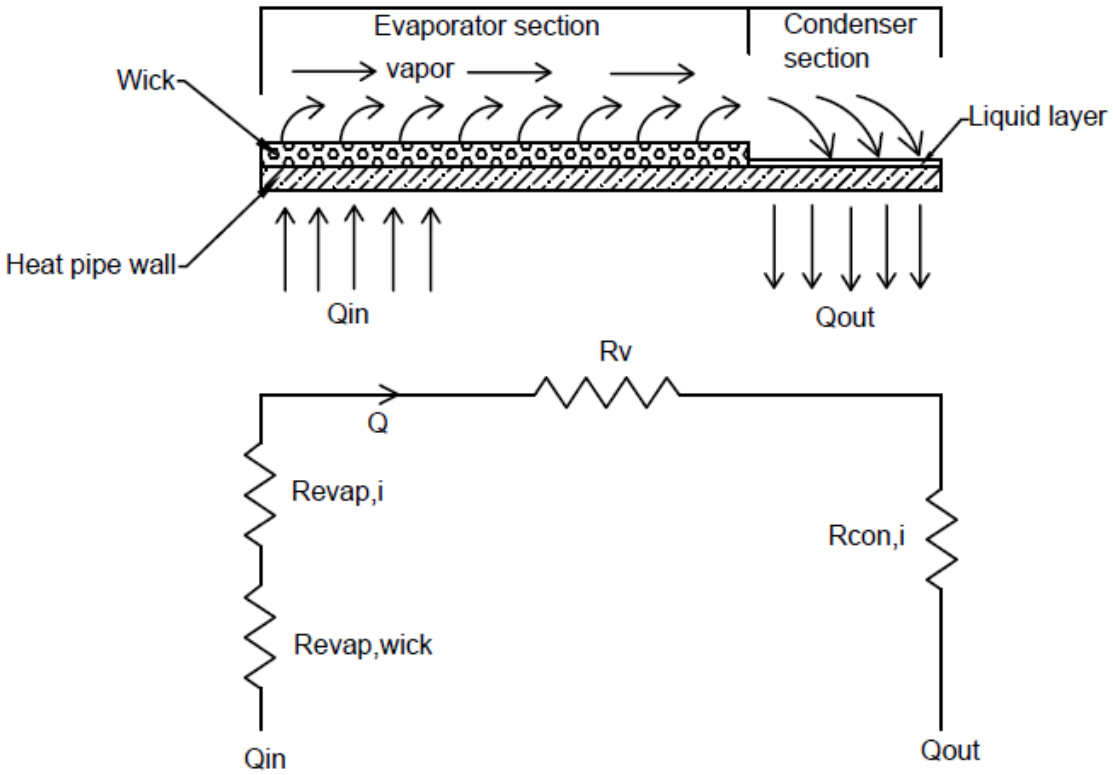

Figure 6: Thermal resistances in the heat pipe

The energy balances for the sensible and latent heat transfer for the water and for the PCM during heating phase includes sensible heating of water and PCM and then latent heat storage of PCM at its melting temperature. The water tank is divided into control volumes each corresponding to the condenser section of the heat pipe and containing equal amount of PCM as shown in Fig. 7.

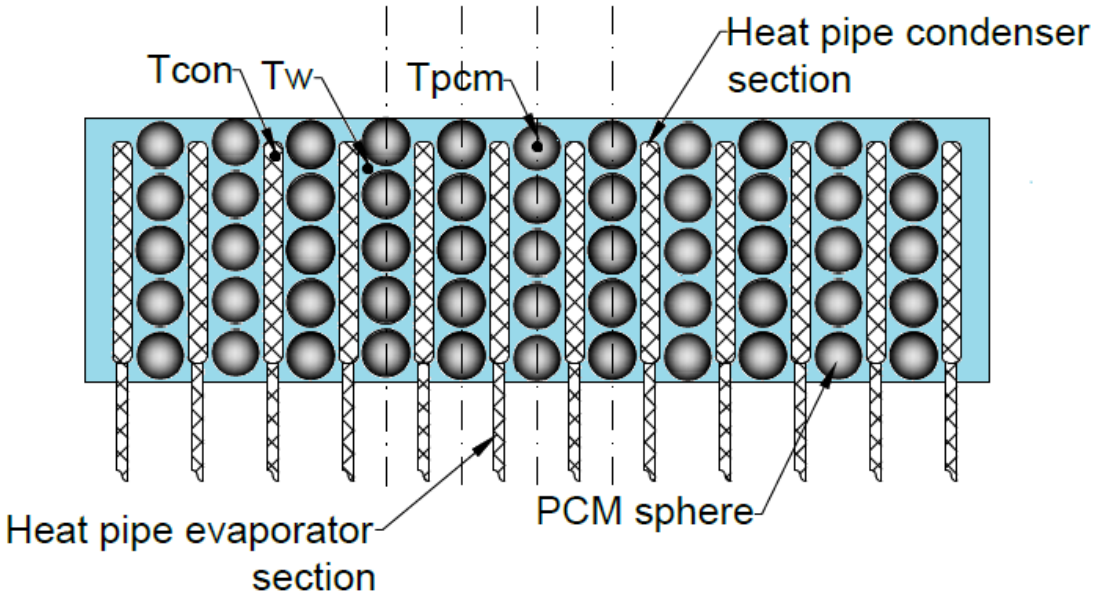

Figure 7: Section of the water storage box

The temperature of water at each control volume is considered uniform (lumped). The corresponding heat balance equation for the water and PCM in each control volume in the storage tank is

$$\rho_w V_w C_w \frac{\partial T_w}{\partial t} = \frac{T_a - T_w}{R_{a,w}} + A_{cond,w} h_{cond,w} \left(T_{p,cond} - T_w\right) + n_{PCM} h_{w,PCM} A_{PCM} \left(T_{PCM} - T_w\right) \quad (7)$$

The first term on the right side of the equation represents the heat loss to the atmosphere. The second term corresponds to the convection heat transfer between the water and condenser in the storage tank. The last term represents the sensible heat transfer between the water and the PCM spheres. $R_{a,w}$ is the equivalent thermal resistance between water and ambient air, A_{PCM} is the surface area of each PCM sphere and n_{PCM} is number of PCM spheres placed in each control volume. $h_{w,PCM}$ is the free convection heat transfer coefficient between the stationary water and the PCM sphere [28]

$$h_{w,PCM} = \frac{Nu_{w,PCM} \times k_w}{D_{PCM,o}}$$

The Nusselt number is determined by the following formula (Incropera et al. [28])

$$Nu_{w,PCM} = 2 + \frac{0.589\, Ra_D^{1/4}}{\left[1 + \left(0.469/Pr_w\right)^{9/16}\right]^{4/9}}$$

where Pr_w is the Prandtl number and Ra_D is the Rayleigh number.

$Ra_D = \frac{g\,\beta_w\,(T_{PCM} - T_w)\,D_{PCM,o}^3}{\nu_w\,\alpha_w}$, with α_w is the thermal diffusivity of water.

The effect of natural convection within the melting PCM is neglected due to small capsule radius and high molten PCM viscosity. The thermal resistance of the capsule wall is assumed negligible since it is very thin and is made of highly conductive material [29-30]. The PCM heat balance equation during sensible heating or cooling is expressed as

$$M_{PCM} C_{PCM} \frac{\partial T_{PCM}}{\partial t} = \frac{(T_w - T_{PCM})}{R_{w,PCM}} \tag{8a}$$

where M_{PCM} is the mass of each PCM sphere, $R_{w,PCM}$ is the thermal resistance between the water and the PCM given by

$$R_{w,PCM} = \frac{1}{h_{w,PCM}\ A_{PCM}} \tag{8b}$$

When the PCM temperature reaches the melting temperature, the PCM starts melting at a constant temperature (T_{PCM}). The PCM stores or releases heat depending on the water temperature. The energy balance equation of the PCM during melting is given by

$$M_{PCM} h_{melting} \frac{\partial X_{liquid}}{\partial t} = \frac{(T_w - T_{PCM})}{R_{w,PCM}} \quad (9)$$

The term to the right side of the equation corresponds to heat transfer between the PCM and water. The parameters $h_{melting}$ and X_{liquid} are the latent heat of fusion and liquid fraction of the PCM, respectively.

B. Numerical Simulation

The resulting energy balance equations are discretized in time and space for the corresponding HP-PV/T panel where it is divided to identical elements for each heat pipe evaporator section with associated fin plate representing one element in the lateral direction *x*. The discretization was only done in the x-direction as the axial temperature variation of the PV panel, base panel and heat pipe along y-direction was neglected because of the uniformity of the heat pipe operating temperature along its axial direction.

The PV panel and the base panel are divided to n elements from *i=1* to *n*. A simple implicit finite difference method is adopted (first order in time and second order in space using central differencing) to solve the coupled equations. At each time step, the Newton-Raphson method is used to obtain an updated value of the solved parameters for the heat pipe and the middle nodes base panel, PV panel, water, and PCM temperatures [12]. The model of Gang et al. was modified to meet our current design were the PCM model was added to the heat sink and natural heat convection heat transfer was considered between the heat pipe condenser section, water and PCM in the PCM tank (heat sink). Initial conditions for the different parameters were taken as

measured experimentally for the PV/T system components while the PCM liquid fraction was set to zero. The output values for the different parameters at the end of an hour system operation are considered to be as the initial conditions of the next hour of operation. The instantaneous boundary conditions included the measured incident solar radiation and ambient temperature and the actual wind speed during the day and night time. Note that along the *x* direction in Fig. 8, the nodes at *i=1* and *i=n* are considered the boundary nodes while all the other nodes are interior nodes. The left and right sides of PV Panel (contain nodes (1) and (*n*)) are adiabatic walls. The methodology for the numerical solution is shown in a flow chart in Fig. 9.

The discretized main heat balance equations are presented as follows and are used to calculate the values for the PV panel temperature, base panel temperature (heat pipe and middle nodes), heat pipe temperature(including the evaporator and condenser), water temperature, PCM temperature and liquid fraction. The superscript 1 represents the value of the parameter at the present instant, while the superscript 0 represents the value of the parameter at the previous time step.

For the PV panel:

$$\delta_{pv}\,\rho_{pv}\,C_{pv}\,\frac{T^{1}_{pv,i}-T^{0}_{pv,i}}{\Delta t}=h_a\,(T_a-T^{1}_{pv,i})+h_{sky,pv}\,(T_{sky}-T^{1}_{pv,i})+\frac{\left(T^{1}_{b,i}-T^{1}_{pv,i}\right)}{R_{b,pv}}+\alpha_{pv}\,G-E_{pv} \quad (10)$$

For the base panel middle node:

$$\rho_b C_b\,\frac{T^{1}_{b,i}-T^{0}_{b,i}}{\Delta t}=k_b\,\frac{T^{1}_{b,i+1}-2T^{1}_{b,i}+T^{1}_{b,i-1}}{\Delta x^{2}}+\frac{1}{\delta_b}\left(\frac{\left(T_a-T^{1}_{b,i}\right)}{R_{b,a}}+\frac{\left(T^{1}_{pv,i}-T^{1}_{b,i}\right)}{R_{b,pv}}\right) \quad (11)$$

For the base panel heat pipe node:

$$\rho_b C_b \frac{T_{b,i}^1 - T_{b,i}^0}{\Delta t} = k_b \frac{T_{b,i+1}^1 - 2T_{b,i}^1 + T_{b,i-1}^1}{\Delta x^2} + \frac{1}{\delta_b}\left(\frac{\left(T_a - T_{b,i}^1\right)}{R_{b,a}} + \frac{\left(T_{pv,i}^1 - T_{b,i}^1\right)}{R_{b,pv}} + \frac{\left(T_{p,evap,i}^1 - T_{b,i}^1\right)}{R_{p,b}}\right) \quad (12)$$

For the heat pipe evaporator section:

$$M_{p,evap} C_p \frac{T_{p,evap,i}^1 - T_{p,evap,i}^0}{\Delta t} = \frac{T_{p,cond,i}^1 - T_{p,evap,i}^1}{R_{evap,cond}} + \frac{T_{b,i}^1 - T_{p,evap,i}^1}{R_{p,b}} \quad (13)$$

For the heat pipe condenser section:

$$M_{p,cond} C_p \frac{T_{p,cond,i}^1 - T_{p,cond,i}^0}{\Delta t} = \frac{T_{p,evap,i}^1 - T_{p,cond,i}^1}{R_{evap,cond}} + A_{cond,w} h_{cond,w}\left(T_{w,i}^1 - T_{p,cond,i}^1\right) \quad (14)$$

For the water storage tank containing PCM

$$\rho_w V_w C_w \frac{T_{w,i}^1 - T_{w,i}^0}{\Delta t} = \frac{T_a - T_{w,i}^1}{R_{a,w}} + A_{cond,w} h_{cond,w}\left(T_{p,cond,i}^1 - T_{w,i}^1\right) + n_{PCM} h_{w,PCM} A_{PCM}\left(T_{PCM,i}^1 - T_{w,i}^1\right) \quad (15)$$

$$M_{PCM} C_{PCM} \frac{T_{PCM,i}^1 - T_{PCM,i}^0}{\Delta t} = \frac{\left(T_{w,i}^1 - T_{PCM,i}^1\right)}{R_{w,PCM}} \quad (16)$$

$$M_{PCM} h_{melting} \frac{X_{liquid,i}^1 - X_{liquid,i}^0}{\Delta t} = \frac{\left(T_{w,i}^1 - T_{PCM,i}^1\right)}{R_{w,PCM}} \quad (17)$$

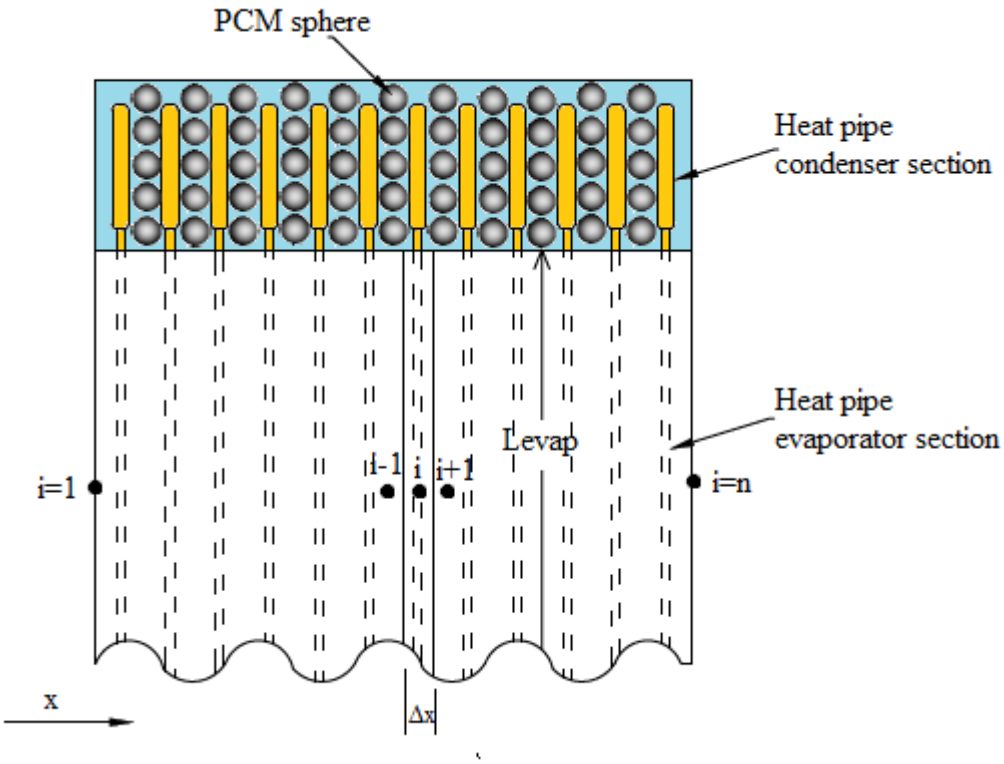

Figure 8: Panel discretization grid

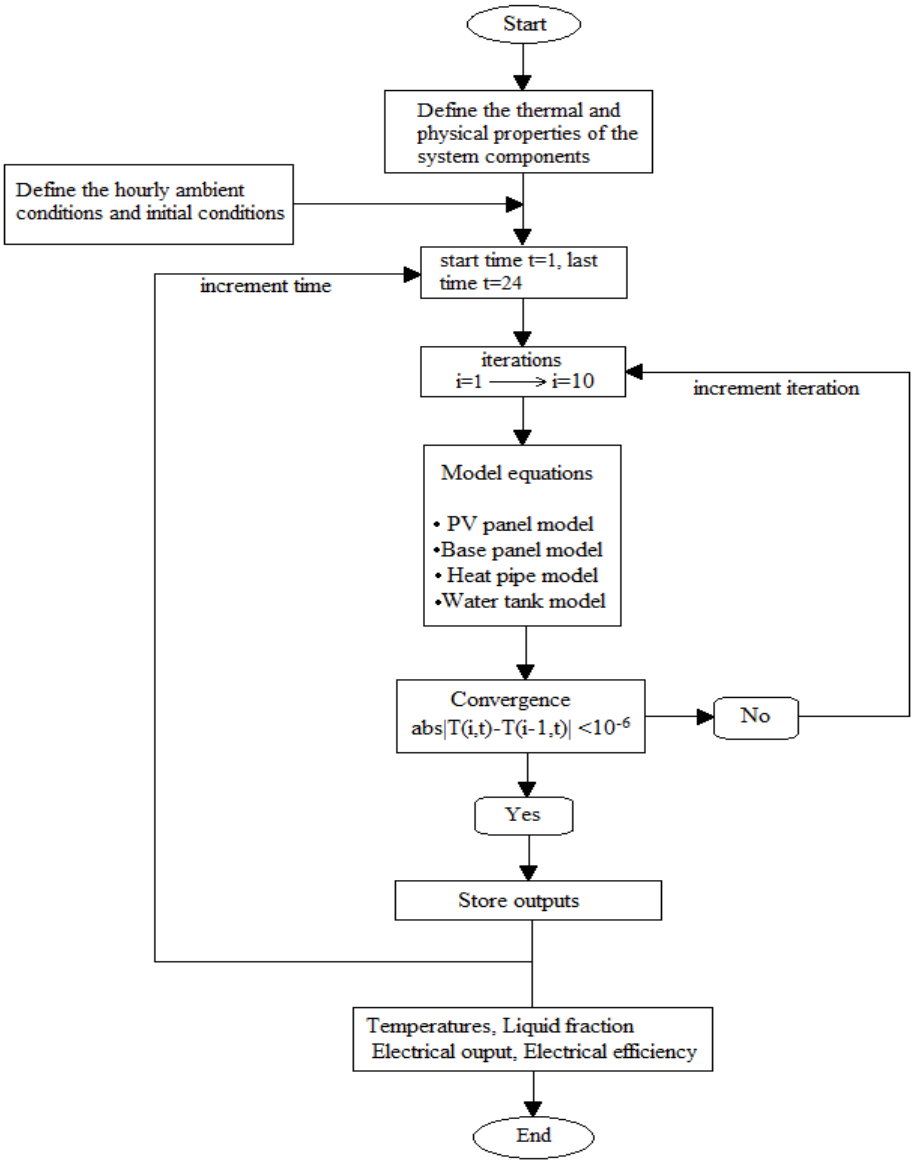

Fig. 4. Flow chart showing the sequence of operation for Simulation

Figure 9: Simulation flow chart

C. Experimental Setup

The experimental setup consisted of the PV panel, water storage PCM tank, and copper heat pipes using dichloromethane as the working fluid. The HP-PV/T system was assembled according to the drawings shown in Fig. 2 and the setup in Fig. 10. An

aluminum plate base panel with an area of 1.64 × 0.98 m^2 and thickness of 7.5 mm was fixed at the bottom the PV panel which has an area of 1.66 × 1.0 m^2 and thickness of 20 mm. A thin layer of high thermally conductive epoxy adhesive layer was applied between the PV module and base panel in order to fill the air gaps and ensure an effective full contact between these components.

The UE 200-M5 PV panel has a peak power of 200W; its voltage and current at peak power are 29.39 V and 6.81 A, respectively and has an operating temperature range of 40°C to 85°C. The decrease in electrical output function of the temperature is estimated by -140mV/°C**.** The PV panel was mounted to be south facing with a tilt angle of 35°, which is almost equal to the location's latitude is 33°54 N.

Twelve copper heat pipes were jointed onto the back of the aluminum plate, and the condenser section was inserted into a PCM-water tank. The PCM-water tank is a rectangular condenser made from 2 mm thick steel plates with an overall dimension of 100 cm × 40 cm × 27 cm. The heat pipe is a hollow evacuated copper tube filled with a liquid refrigerant. The heat pipe has a smaller diameter section (φ15 ×1×1640 mm) representing the evaporator section, in which the refrigerant is heated and transferred by buoyancy to the upper condenser section of the pipe having a larger diameter (φ25 ×1×400 mm). These dimensions were chosen to have equal evaporator and condenser volumes of the heat pipe, with a larger condenser diameter to increase the surface area and allow for efficient condensation of vapor. A thin steel wire mesh (wick) was rolled and fitted within the inner radius of the pipe, allowing for quicker movement of the evaporated particles of the working fluid as condensed droplets attach to the wire mesh The porosity of the wick was 0.6 with a mesh number *m=14*, wire diameter *d*= 0.89 mm

and the opening width of mesh w=0.6 mm. Each pipe was evacuated to 0.7 bars and filled with a quantity of 215 ml (filling ratio was 0.85 of the evaporator volume) by the selected refrigerant (dichloromethane). A filling ratio equal or greater than 85% of volume of evaporator was reported to have better results in terms of increased heat transfer coefficient, decreased thermal resistance and reduced temperature difference across the evaporator and condenser [31]. The space between the two adjacent heat pipes was 66 mm.

The PCM used in the experiments were made of salt hydrate contained in spherical capsule having an outer diameter of 75 mm and made high-density polyethylene (HDPE) with a wall thickness of 0.7 mm. Each PCM sphere has a mass of 311.5 grams with density of 1400 kg/m^3 and a melting temperature of 29^{o}C. The PCM specific heat of fusion is 211.66kJ/kg with specific heat of solid and melting phases of 2,900 J/kg·K and 2,130 J/kg·K, respectively. Sixty PCM spheres having a total volume of 0.0314 m^3 and a total mass of 18.69 kg were placed inside the storage tank containing 75 L of water.

The thermal properties for the different materials used in the system are summarized in Table 1. The base panel with the exposed area of the heat pipes was insulated with fiberglass and a layer of reflective aluminum. The water tank was covered with a layer of reflective aluminum that prevents the absorption of the solar radiation during the day while it allows for excess energy dissipation from the tank to the atmosphere during the night. The experiment was done during the first week of July in Beirut City. The global solar insolation (direct and diffuse radiation) was measured using a global pyranometer that was positioned on the panel's surface and has a

sensitivity of 15×10^{-6} Volts/(W/m²) and a maximum accuracy of ± 3 % for temperature range between -10°C to +40°C. Weather data including the ambient temperature and solar radiation were monitored and recorded for every hour during the experiment. Type K thermo-couples with accuracy of ±0.1°C to 0.5°C were used to measure the temperatures of the PV panel, hot water and PCM surface over a 24-hour period. A rheostat was used to measure the power output of the PV panel (with and without heat pipes).

Monitoring devices for temperature and solar radiation were installed at different locations as was shown in Fig. 2. These devices included two Fluke 115 multi-meters for measuring the current and voltage at accuracies of 1.0% and 0.5%, respectively. The data logger for monitoring outdoor ambient temperature and humidity had accuracy of ± 1.0°C and ± 3%, respectively. Thermocouple 1 was used to record the PV panel surface temperature, while thermocouples 2 and 3 recorded the hot water and PCM surface temperatures, respectively. The experiments were performed at the end of June and beginning of July and the final data presented later refer to 3rd of July, where the experiment started at 1 a.m. and measurements were taken over a 24 hours period.

Table 1: Thermal properties of different system materials

System Component	Material	Thermal conductivity (W/m·K)	Density (kg/m^3)	Specific Heat (J/kg·K)
PV panel	Mono crystalline silicon	148	2,329	731
Base Panel	Aluminum	237	2,702	903
Heat pipe	Copper	401	8,960	385
Wire Mesh	Stainless Steel	17	8,060	530
Water tank	Steel	60.5	7,845	434

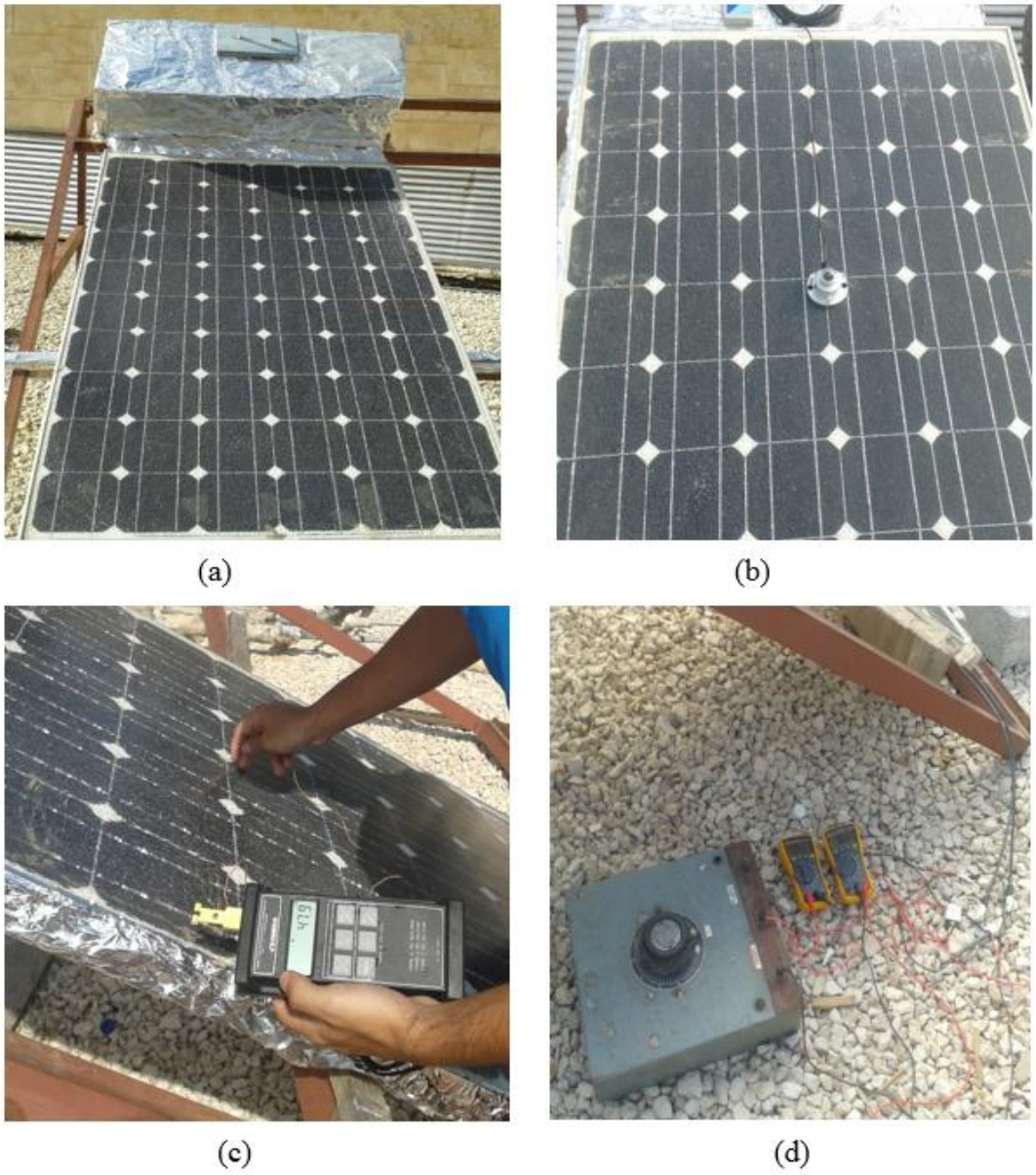

Figure 10: Photos of the experimental setup showing (a) the system assembly (b) global pyranomoter (c) Rheostat and (d) thermo-couple for measuring the PV panel temperature

D. Results and Validation

The recorded weather and solar data and the geometric and physical parameters of system components (PV, Heat pipe, PCM, and tank) were used as input to the integrated simulation model. The experiment was started from an approximately

uniform initial water and PCM temperatures of 25.2ºC according to the readings of the thermocouples located inside the tank. The measured initial temperatures of the PV/T panel and Standard PV panel were 25.1ºC and 24.4ºC respectively. These temperatures were used as input for the model simulation at the beginning of the first hour. The measured hourly values of ambient temperature and the global solar radiation during the experiment (3rd of July) are presented in Table 2. The model predictions are compared to the experimentally measured values of temperatures of the PV/T panel, water, and PCM and to the measured electrical gain of the HP-PV/T.

Table 2: The hourly measured values of ambient temperature and the global solar radiation during the experiment (3rd of July)

Hour	Hourly ambient Temperature (°C)	Hourly solar radiation (W/m^2)
1	25.0	0
2	24.8	0
3	24.7	0.0
4	24.5	0.0
5	24.6	0.0
6	25.3	2.4
7	26.3	48.4
8	27.5	175.4
9	29.2	363.9
10	31.0	543.9
11	32.3	707.0
12	33.4	814.7
13	33.5	835.7
14	32.4	769.5

15	31.3	618.4
16	30.0	451.3
17	29.3	264.9
18	28.8	106.9
19	28.0	24.7
20	27.0	0.0
21	26.3	0.0
22	26.0	0.0
23	25.8	0.0
24	25.6	0.0

Figure 11 shows the experimentally measured and model prediction of the PV panel temperature for two PV/T panel and standard PV panel. For both cases, the temperature of the PV panel started rising in the morning (6 a.m.) until it reached the maximum at 1:00 p.m., then it dropped for the rest of the afternoon. The maximum temperature of the panel surface for standard PV panel was 63.33 °C occurring at 1:00 p.m. while the maximum PV/T surface temperature reached 48.4 °C at 1:00 p.m., dropping by 14.9 °C at the peak hour compared to standard PV. During the night, the temperature of the PV/T panel was higher than that of the standard PV panel because it was insulated from below and thus less heat is dissipated to the environment. It is evident from Fig. 11 that good agreement was attained between the model prediction and experimental data with a maximum percentage error of 7.4% and 6.9% for the PV temperature with and without heat-pipes, respectively. The maximum error observed near the initial conditions decreased gradually after some period of time when the effect of the initial conditions became insignificant. The errors between the simulation and

experiment resulted mainly from the model assumption of uniform PV panel temperature along the axial direction of the heat pipe.

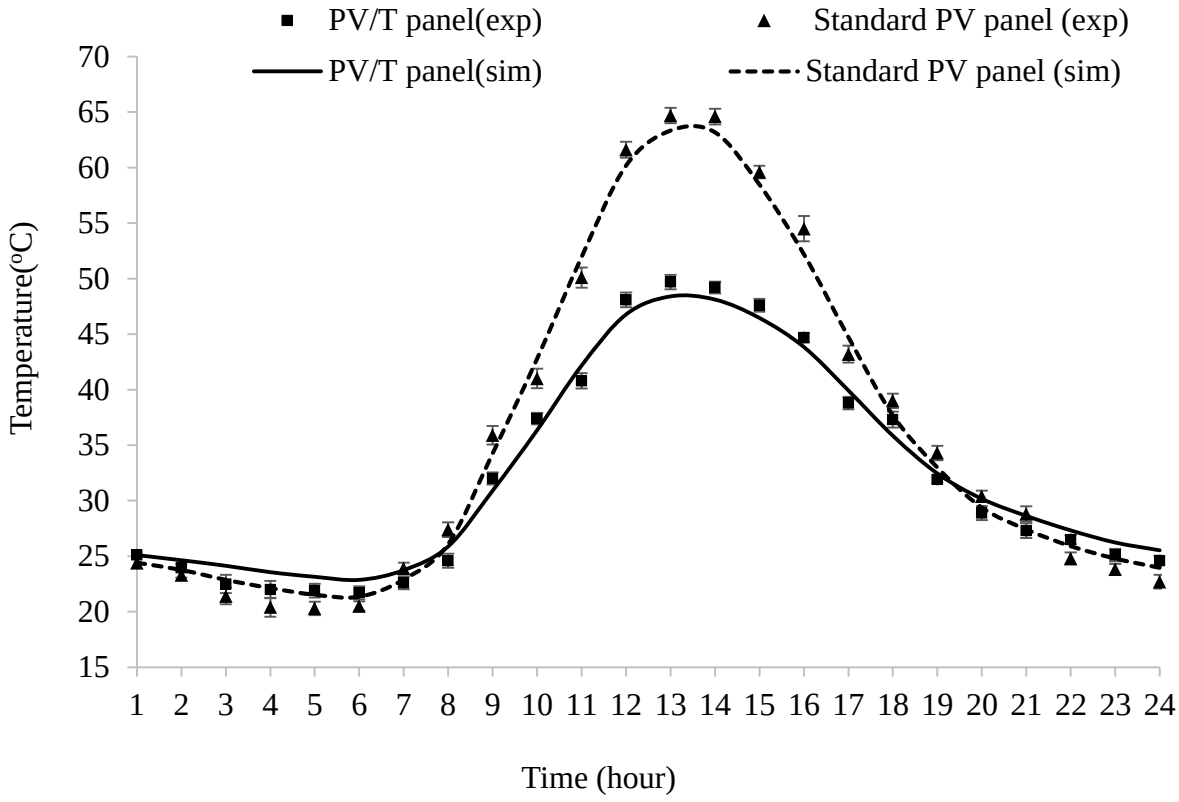

Figure 11: Plot of the PV panel temperature for PV and HP-PV/T-PCM systems

Figure 12 shows the variation of (a) the water temperature and (b) the PCM temperature in the storage tank. The temperature of the water increased with the increase of the solar irradiance until the PCM started melting in the water tank when water temperature reached 29 °C at around 10:30 am and stabilized at a nearly constant temperature until the PCM completely changed phase from solid to liquid at about 1:30 p.m. The PCM kept a nearly constant water temperature during the peak hours and provided a suitable heat sink for the heat pipes' condenser. When the PCM melted

completely, a further sensible increase in the water and PCM temperatures was observed between 3:00 pm and 5:00 p.m. The predicted melted mass fraction of the PCM is also plotted in Fig. 12(b) which clearly shows the time when melting starts in the morning at about 10:30 am and when solidification starts at night at about 11 pm. During the night (after 10 p.m), the PCM maintained an almost constant water temperature (Fig. 12). It is clear from both graphs that a slight temperature difference appears between the water temperature and the PCM temperature. During the early hours of the experiment, both temperatures started decreasing simultaneously with the water temperature being slightly lower than that of PCM. The PCM temperature change is found to be very sensitive to the change in the water temperature. This is due to the fact that water acts as a conduction medium between the ambient environment and the PCM while the PCM has a low equivalent heat capacitance when being in the solid state compared to that of water. As the solar radiation increases during the day, more heat reaches the PCM tanks through the heat pipe condensers. This energy is transferred to the PCM spheres through water (being at a slightly higher temperature than that of PCM). When the PCM temperature reaches the melting point, the PCM starts melting at a constant temperature (29^{o}C) while storing heat in the latent form. However, the water temperature continues to increase slightly because its equivalent heat capacitance is lower than of the PCM during phase change. When the PCM totally melted (1:30 p.m.) both temperatures showed a further increase, with the PCM temperature increase trend being similar to that of water because of the low equivalent heat capacitance of the liquid PCM compared to that of water. Then, both temperature dropped until 11 a.m. where the PCM started melting and releasing heat to water being at slightly lower temperature.

The experimental data were in good agreement with simulation results of tank and PCM temperatures with a maximum deviation of 7.2%. The errors are mainly caused by the lumping assumption of the water and PCM temperatures and the assumed uniformity of temperature at all positions of the PCM during the melting phase. The case of HP-PV/T when no PCM was used in the water storage tank for the same experimental setup was simulated and the expected water temperature was plotted in Fig. 12(a). The predicted water temperature increased significantly without PCM reaching 42 °C at the peak hour.

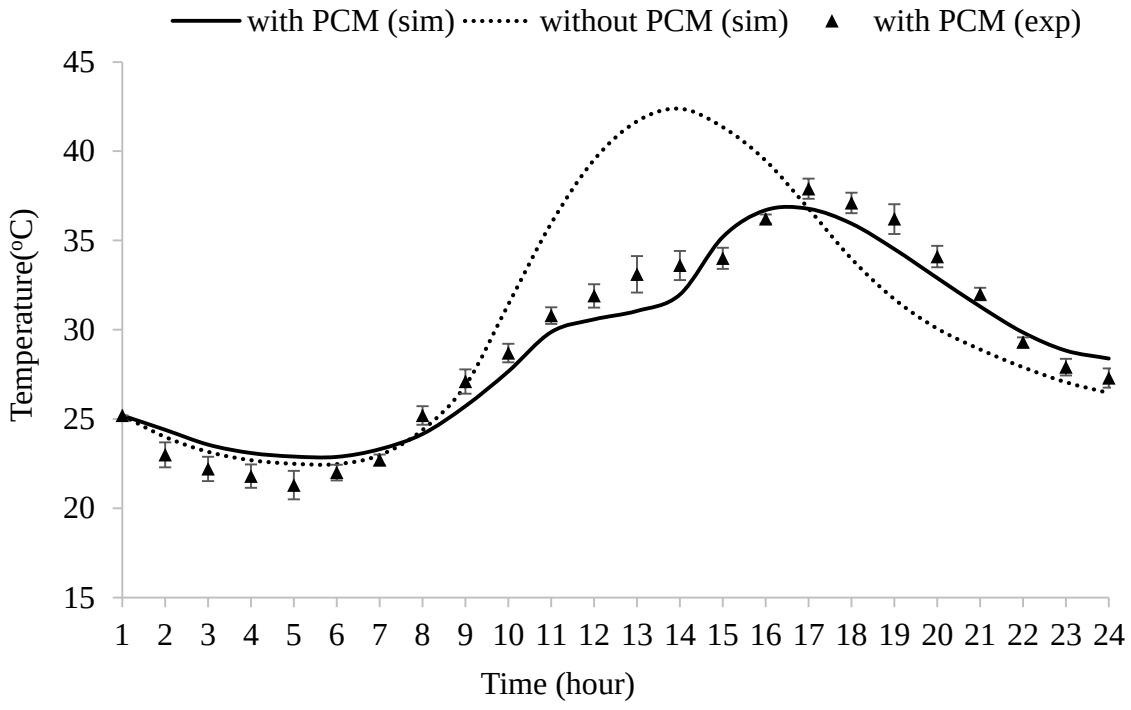

(a)

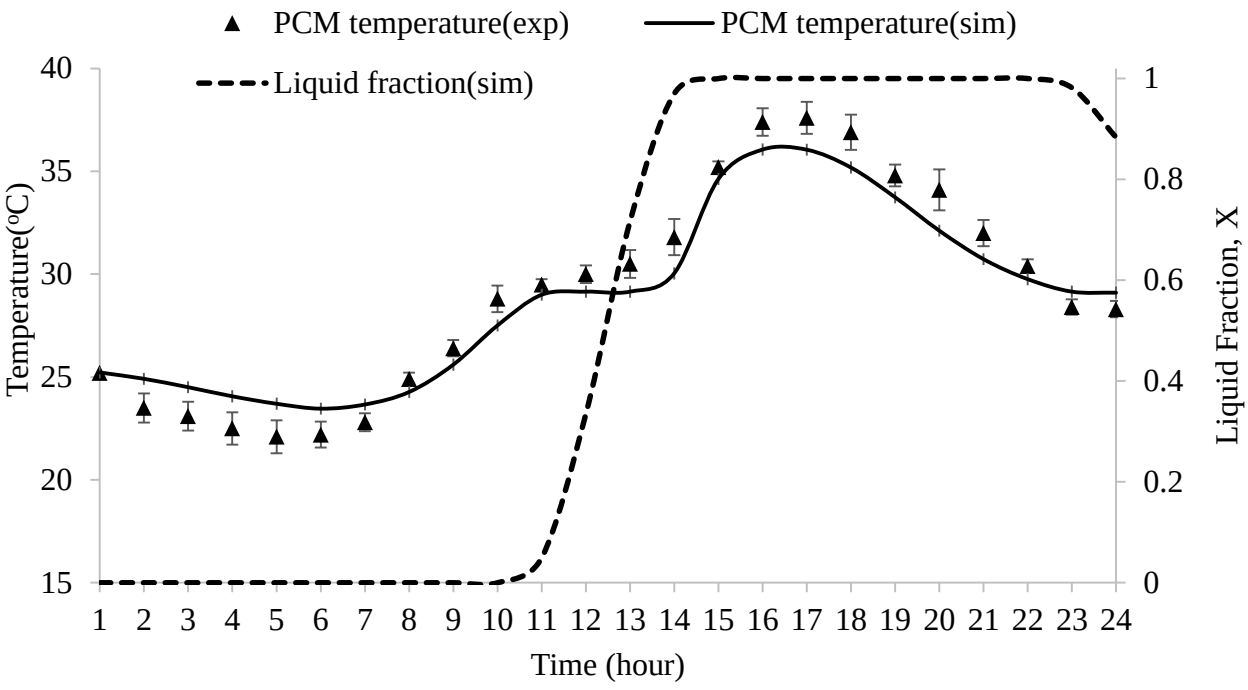

(b)

Figure 12: Plots of the time variation of (a) predicted and experimentally measured water temperature and (b) predicted and experimentally measured PCM temperature in the storage tank as well as the predicted PCM melting fraction

The measured and predicted electrical gain per unit PV area and the corresponding electrical efficiency are plotted respectively in Fig. 13(a) and Fig. 13(b) for both the standard PV panel and the HP-PV/T-PCM panel. For the standard PV panel, the electrical gain reached a maximum of 79.85 W/m^2 at the peak with an electrical efficiency of 9.44%. However, when the heat pipes were used to cool the PV panel, the electrical gain reached a maximum of 86.3 W/m^2 at 1 p.m. with an electrical efficiency of 10.29%. After that, the electrical gain decreased gradually with decreased solar radiation. The use of HP-PCM combination resulted in 9% improvement in the PV module's electrical efficiency at peak conditions, which is comparable with the photovoltaic/thermal systems studied by Wu et al. [11] and Gang et al. [12]. In addition,

good agreement was found between simulation results and experimental data of electrical gain where maximum deviations observed were 7.72% and 6.83 % for the PV/T panel and standard PV panel, respectively.

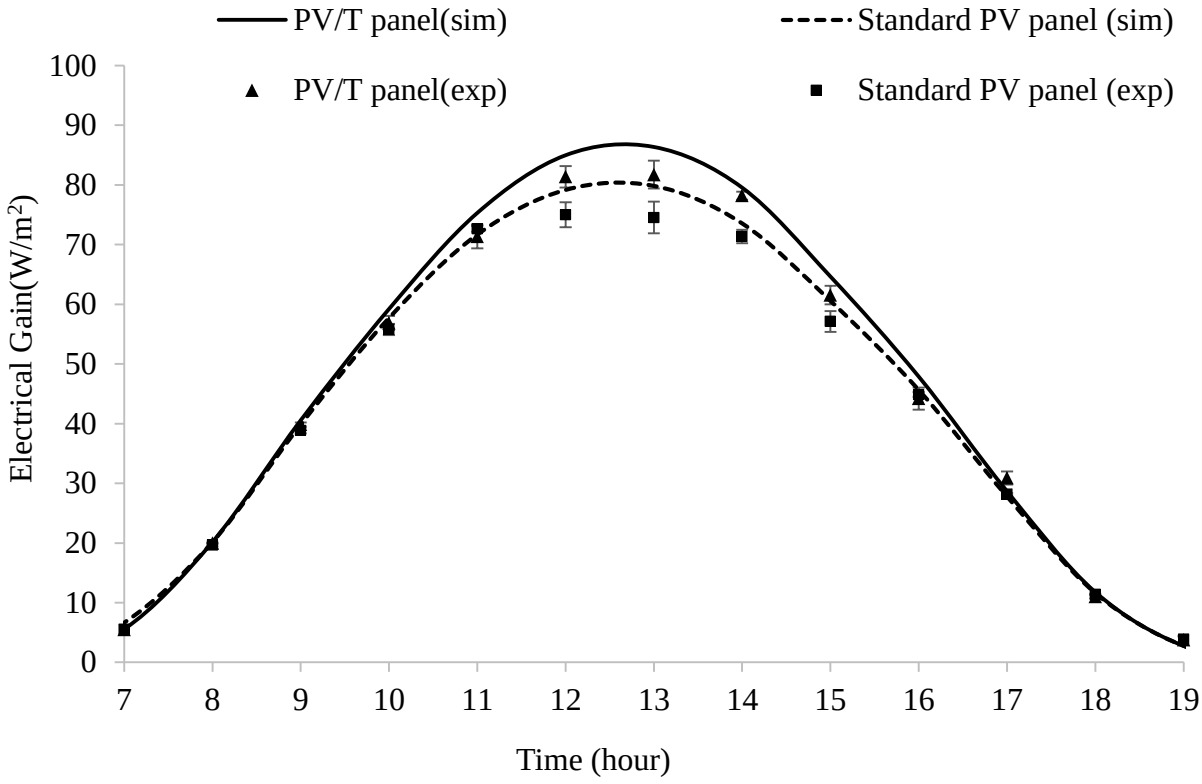

(a)

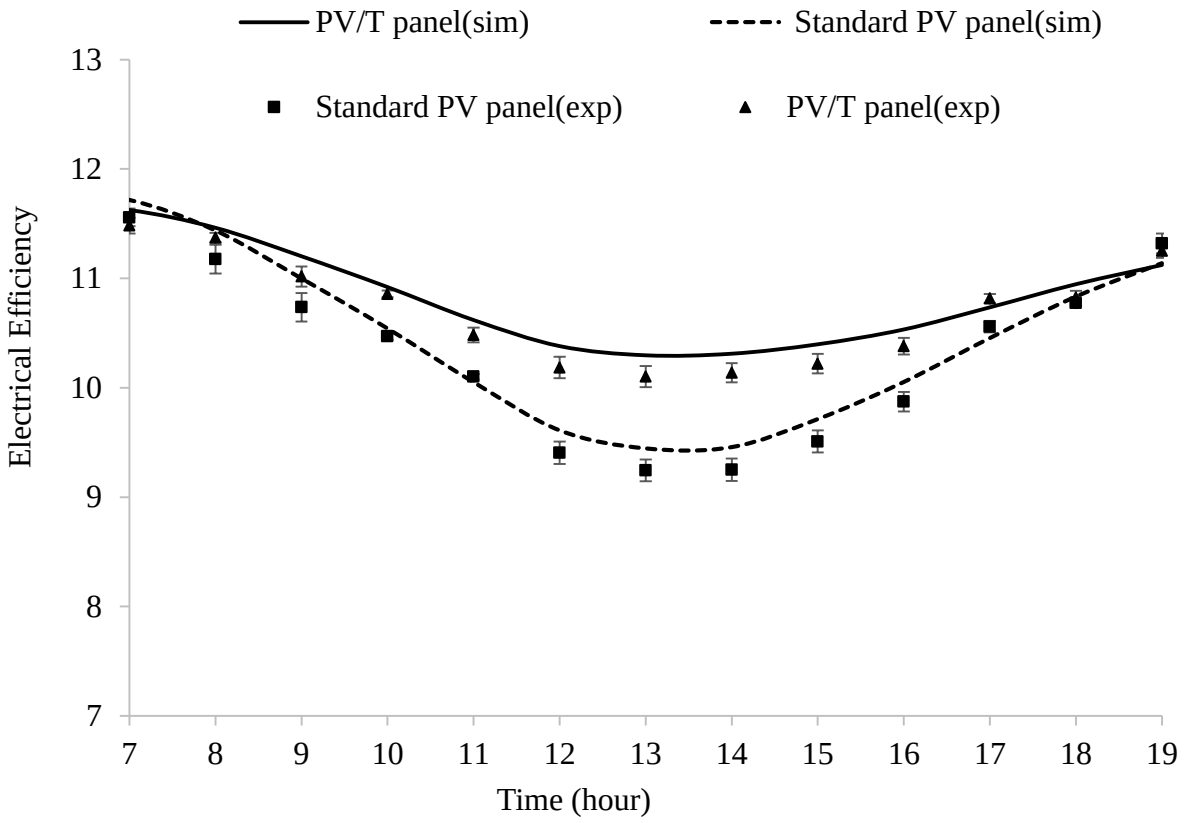

(b)

Figure 13: Plots of measured and predicted (a) electrical gain and (b) electrical efficiency versus time for standard PV panel and HP-PV/T-PCM panel

CHAPTER IV

OPTIMIZATTION OF THE OFFICE-INTEGRATED HP-PV/T-PCM SYSTEM

A. System Integration and Optimization

The existence of multiple subsystems in the HP-PV/T-PCM system (see Fig. 14) requires performing design optimization to ensure the design that meets the electrical energy consumption while minimizing the thermal energy needs for heating water throughout the year with smallest PV area and minimum acceptable number of PCM spheres in each HP-PV/T-PCM tank. Optimization is applied to a case study of an office space in Beirut climate (refer to Fig. 14).

Optimizing the HP-PV/T-PCM system is a complex task since we are dealing with a system of integrated multi-models and a set of non-linear equations, so it is preferred to use a derivative free optimization tool that works according to the direct search principle. For this purpose, the genetic algorithm (GA) tool is used because it is efficient for optimizing systems where indirect relations between the different parameters exist [32]. Genetic algorithm is a quick and simplified technique characterized by fast convergence in obtaining a good enough solution and in searching for combinations of parameters that improve the performance [33-34].

The Genetic Algorithm terminology is described by the following steps:

- The algorithm starts by seeding a set of trial combinations of the variables to be optimized and calculating the numerical value of the objective

function for each combination selected. This set is called the "*Initial Population*".

- The set of numerical values calculated for the objective function from the first trial, is then evaluated according the "*Fitness Criteria***"**. The fitness criteria can be defined as the condition for the objective function numerical value to be better convenient than its pears.
- Based on their fitness, some combinations in the previously seeded set are chosen to be "**Parents".** Parents then undergo either "*Crossover***"** or "*Mutation***"** procedure to produce "**Children**". Most fitted parents simply jump to the next generated population without any change; such parents are referred as "*Elite***"**.
- The current population is replaced by children from the next population.
- **Elite children** are the individuals in the current generation with the best fitness values. These individuals automatically survive to the next generation. *Crossover children* are created by combining the vectors of a pair of parents. *Mutation children* are created by introducing random changes, or mutations, to a single parent.
- The algorithm stops when the "*Tolerance*" in the objective function values between two generations is less than a certain set error value, or when the maximum number of **"Generations"** is exceeded, or by any other defined **"***Stopping Criteria***"**.

The Genetic Algorithm procedure implemented in this work is summarized as follows:

1. Randomly initialize a population of individuals, such that each individual represents the random combination of the design variables. The population used is 20 times the number of variables.
2. The objective function is calculated for each individual.
3. The fitness of each individual is then evaluated using the information from the objective function.
4. The individuals are sorted by their fitness using the Rank Selection.
5. The best individual is saved as elite member so that it will continue to exit in the next generated population. The elite count represents the number of individuals with the best fitness values in the current generation that are guaranteed to survive to the next generation. An elite count of 2 is chosen because setting the elite count to high values causes the fittest individuals to dominate the population, which make the search less effective.
6. Now the top individuals are selected to be parents for reproduction.
7. A couple of parents from the selected individuals are randomly chosen for the reproduction process.
8. New children are generated by crossover and mutation. Scattered cross over is used with a cross over fraction of 0.2. The cross over fraction determines the fraction of individuals in the next generation, other than elite children that are created by cross over. Mutation children are created by introducing random changes, or mutation, to a single parent.
9. The elite member and the new children represent the next generated population.

10. The GA continues to reproduce new generations until the *"Tolerance"* between two generations is less than a certain pre-set error value. In this work the function tolerance is 1×10^{-6}.

The system design variables that are optimized are: i) the number of PV Panels (placed in a parallel configuration); ii) the amount of PCM spheres needed in each PCM tank; and iii) the melting temperature of the PCM. The size of the PCM storage tank is determined according to the minimum amount of PCM required. The water tank for each PV/T panel will be sized to have the highest packing density of PCM spheres consistent with the work of Yang et al. [29] and Ledesma et al. [30] to maximize the capture of latent energy [35], while the water acts as a heat conducting medium between the PCM spheres. A circulation pump is used to circulate water that transfers heat from the HP-PV/T-PCM tanks to the storage tank, whenever the HP-PV/T-PCM tanks' temperature in the PV/T modules is higher than the storage tank water temperature (see Fig. 14).

A modified design of the PCM tank includes heat exchange tubes for extracting heat as shown in Fig. 14. The temperature of the hot water leaving the PCM tanks ($T_{w,out}$) and entering the storage tank is calculated by considering the case internal forced convection inside an isothermal tube at the lumped water temperature($T_{w,tank}$) [28]. The tube is assumed with enough passes inside the HP-PV/T-PCM tank to ensure an effectiveness ε=0.85.

$$T_{w,out} = T_{w,tank} + \varepsilon \times \left(T_{w,in} - T_{w,tank} \right) \tag{18}$$

where, $T_{w,in}$ is the inlet water temperature.

The water temperature in the storage tank is determined using a fully mixed tank model [36]. An auxiliary heater will be used when the water supply temperature to the office is less than desired level during the hours of system operation.

The optimal values of the above stated variables should concurrently ensure that the HP-PV/T-PCM system provides hot water while using the minimum auxiliary heating energy possible and meeting the annual electrical energy needs at zero cost. The objective function *J* represents the total system cost over its life time including the cost of heat, cost of cooling system incremental cost of HP and cost of PCM and is written as follows:

$$J = J_{aux} + N_{PVT} \times C_{PVT} + N_{PCM} \times C_{PCM} \tag{19a}$$

J_{aux} is the total of the yearly cost of the auxiliary energy needed for heating water over the life cycle of the system, and is defined as

$$J_{aux} = \sum_{i=1}^{N} \frac{C_{aux} \times J_{auxiliary\text{-}heat}}{(1+a)^i} \tag{19b}$$

where a is the discount rate, *N* is the life time of the system and $J_{auxiliary\text{-}heat}$ is the yearly running cost[kWh] for year *i* and is given by

$$J_{auxiliary\text{-}heat} = \dot{m}_{w,office} C_w \left(T_{w,office} - T_{w,storage} \right) \tag{19c}$$

$J_{auxiliary\text{-}heat}$ [kWh] is calculated based on the hot water consumption supply flow rate ($\dot{m}_{w,office}$) whenever the temperature of water leaving the storage tank ($T_{w,storage}$) and supplied to the office is lower than the needed hot water temperature of the office, $T_{w,office}$ ($T_{w,storage} < T_{w,office}$). C_{aux} represents the cost of auxiliary heating [$/kWh]. N_{PVT} is the number of PV/T panels required to meet the electrical needs of the office based on

the below explained constraint and C_{PVT} represents the cost of the PV/T panel incremental cost over standard PV panel. N_{PCM} is the total number of PCM spheres used in the system and C_{PCM} represents the cost of one PCM sphere. The life time span of the system is taken as *N=25 years* for cooling the PV panel with PCM [37-38-39]. The constraints that will be observed when performing the optimization are summarized as follows:

- The circulating pump in the closed loop between the HP-PV/T-PCM modules and the storage tank (refer to Fig. 14) operates during the working hours whenever the water temperature, T_w, in the PCM tank is higher than that in the office storage tank ($T_{w,tank}$) ($T_w > T_{w,tank}$). In addition, the temperature of the water leaving the storage tank and entering the PCM tank, $T_{w,in}$, must be lower than the lumped temperature in the PCM-tank ($T_{w,in} < T_w$) for efficient heat removal; otherwise the circulating pump will be OFF.
- The optimization aims is to find the minimal amount of PCM that provides the maximum heating for water in the storage tank while insuring complete solidification during night hours in all seasons. To enhance heat dissipation, the PCM-tank is not insulated. This allows the PCM tank to lose heat to the environment at night and ensures complete solidification of the PCM spheres (X_{liquid}=0 before 6 a.m.) to initialize the system operation for the next day cycle [34]. Accordingly, the melting point of the PCM should be higher than the night air temperature to prevent the energy build up and accumulation from day to day in the PCM tanks, thus protecting the system from overheating [37].

– In sizing the PV panels, the total of the electricity generated by the PV/T panels must be equal to that consumed throughout the year. The hourly electrical energy bought from or sold to the grid J_{elec} [kWh] for an on-grid system is given by

$$J_{elec} = J_{PV} - J_t = J_{PV} - \left(J_{office} + J_p \right) \tag{20a}$$

where J_t *is* the total electrical energy consumed by the office's equipment (J_{office}) and the system pump (J_p) [kWh] and J_{PV} is the electrical energy produced by the PV panels [kWh]. The electrical energy consumption of the system circulating pump is expressed by

$$J_p = \frac{\gamma_w Q_w H}{\eta_{pump}} \tag{20b}$$

where, γ_w and Q_w are the specific weight and volumetric flow rate of water respectively. H is the head loss for the current system and η_{pump} is the pump efficiency and has a typical value of 85%. The yearly J_{elec} (presented in eq. 10(a)) must be greater than zero ($J_{elec,yearly} \geq 0$) to insure that the number of PV panels is able to meet the electrical need. The electricity is sold and bought at the same price, however in performing the optimization, any excess yearly electric energy produced will have zero value since the objective is to meet the electrical needs (zero net electrical power balance) and minimize the auxiliary heating cost with the minimum number of PV panels and PCM spheres.

The methodology for the optimization is shown in the flow chart in Fig. 15. The useful heating energy supplied by the HP-PV/T-PCM panels to the office water storage tank is defined as

$$Q_w = \dot{m}_w C_w \Delta T \tag{21a}$$

Where $\dot{m}_w$ is the mass flow rate of the circulating water and ΔT is the temperature difference between the circulating water entering and leaving the office storage tank.

The thermal efficiency defined as the ratio of the water heating energy supplied by the HP-PV/T-PCM panels to the total radiation received by the panels is given by

$$\eta_{thermal} = \frac{Q_w}{G \times A_{pv} \times N_{PVT}} \tag{21b}$$

Since electricity is high grade energy that it is converted from thermal energy, while the heat energy produced at nearly environmental temperatures is a low grade energy, it is necessary to convert the electrical efficiency of the PV cells to an equivalent thermal efficiency for a thermal power plant when evaluating the total equivalent thermal efficiency of the HP-PV/T-PCM system (η_{pvt}), where it is expressed as [4]

$$\eta_{pvt} = \eta_{electrical} / C_f + \eta_{thermal} \tag{21c}$$

with C_f representing the conversion factor of the thermal power plant and is taken equal to 0.38 [40].

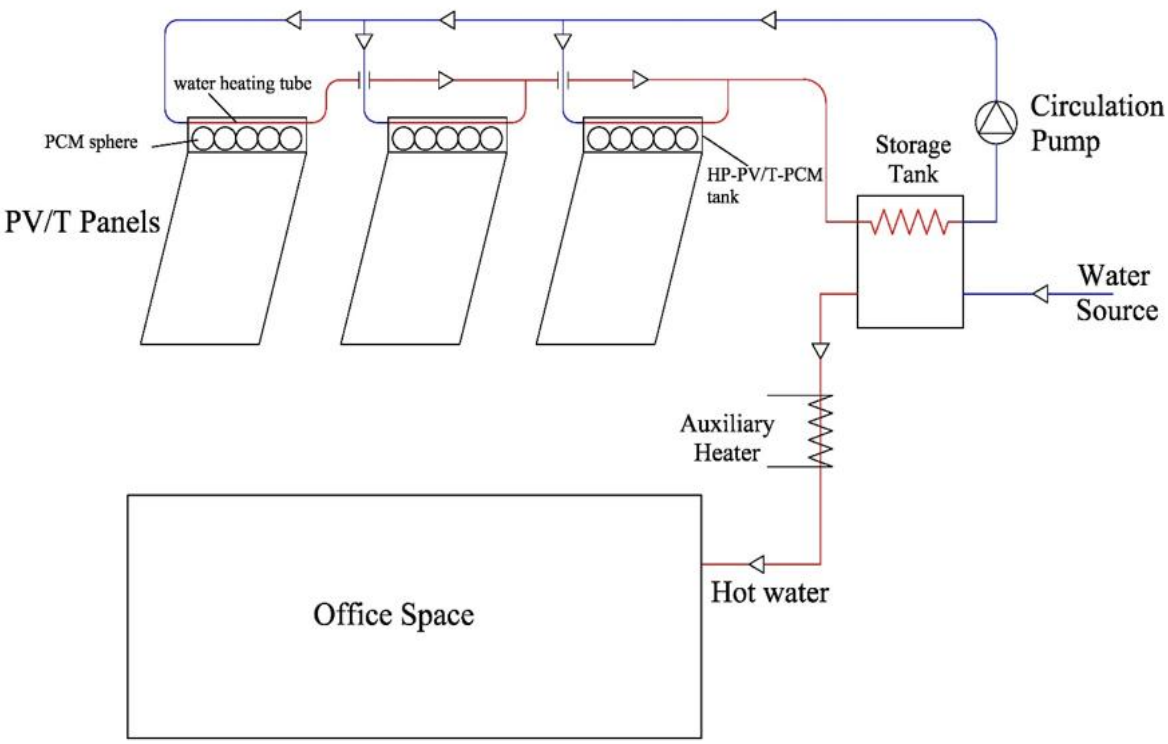

Figure 14: Schematic of the HP-PV/T-PCM office integrated system

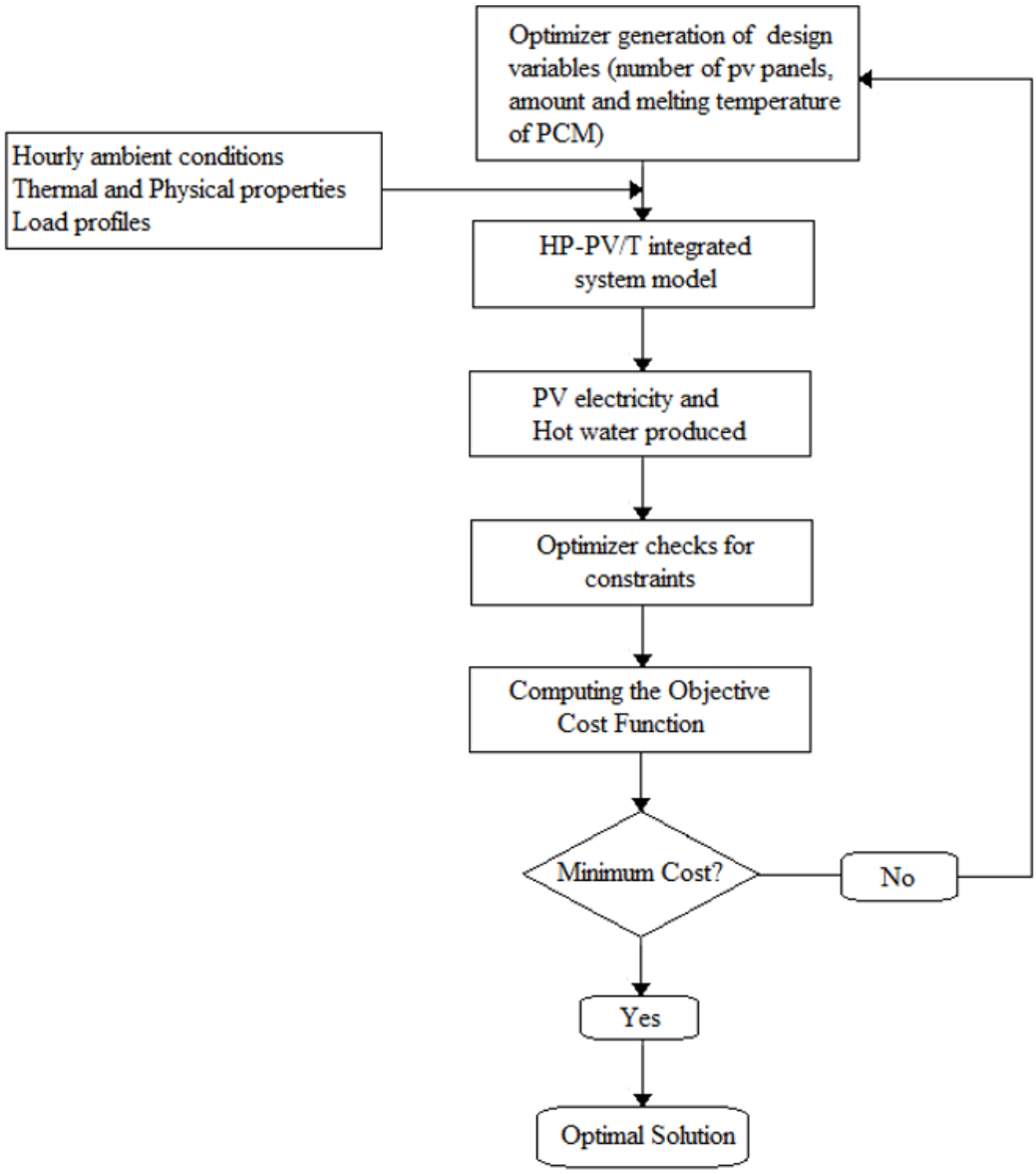

Figure 15: Flow chart showing the sequence of operation for Optimization

B. Case Study

1. System Description

The HP-PV/T-PCM system shown in Fig. 14 is implemented for a typical office space in Beirut to cover the electrical and domestic hot water needs. The electricity needs for computers and lighting is to be supplied by the PV system without electricity storage (on-grid system). The extracted heat from the HP-PV/T panels is used to heat up domestic water before being supplied to the office. The office has overall dimensions of 8m × 8m ×3m and it is occupied by 5 people from 7:00 a.m. till 7:00 p.m. It includes 5 desktop computers each requiring 150W, and the lighting load is assumed to be 11W/m^2. The total electrical load of the office equipment is 14.92 kWh/working day all year around according to the ASHRAE Standard 90.1 [41]. The DC/AC converter efficiency is assumed 95%, and additional electrical losses of 10% are considered. Hence, the electrical power to be provided to the office equipment by the PV panels is 1.45 kW. The hot water is to be supplied at minimum temperature of 32^{o}C according to a schedule [42] (refer to Table 3) based on a daily consumption of 22 liters/day for each occupant [43]. According to the Food Code by the U.S Department of Health and Human Services [44], the hand washing hot water should be available at a range of 40° ±3°C so that employees could mix with cold water. However in our case, the hot water temperature of 32^{o}C was chosen considering that this water is used directly without mixing with cold water. The circulating water pump power consumption is added to the office electric energy consumption based on the hours of operation of the pump that circulates water at a rate of 0.45 kg/s as used by Gang et al. [12] for the case of the PV/T panels (0.09-0.092 L/s for a PV/T system of 4 collectors each having an

area of 1.5m^2) and by Garg et al. [45] who found that a mass flow rate 0.03 Kg/s will provide the best total efficiencies for a PV/T collector of 2m^2 area. The auxiliary heater is used in case the temperature of hot water supplied by the HP-PV/T-PCM system is below 32^oC. In this study, the working refrigerant fluid used in the heat pipes of the PV/T panels is Methyltetrahydrofuran (2-MeTHF).

Table 3: Hourly hot water consumption profile [42-43]

Hour	Hot water consumption (liters)
7-8	14
8-9	11
9-10	5
10-11	5
11-12	7
12-13	15
13-14	13
14-15	5
15-16	5
16-17	7
17-18	8
18-19	15

2. Results and Discussion

In order to simulate and optimize the operation of the integrated HP-PV/T-PCM system, the optimization procedure was performed over a whole year. A representative day (21^{st}) for the solar and weather data is chosen for each month of the year [46]. The inputs for the simulations include: the physical and thermal properties of the different components, the occupancy and equipment electrical consumption profile, the solar and weather data, hot water consumption profile assuming that the replacement water coming from the mains enters the storage tank at an average temperature equals to the average ground temperature[47] for each month. The optimizer chooses a number of HP-PV/T-PCM panels and sets an amount of PCM at a specific melting temperature. Then, it calculates the daily and yearly electricity produced, the temperature of the hot water produced, and the auxiliary heat needed while checking for the constraints. Finally, the cost function is calculated for the selected set of variables, and the procedure is repeated until the optimal values of the variables minimizing the cost function are obtained. The sequence of optimization steps is summarized in Fig. 15.

When performing the optimization, each variable must be defined by a lower and upper bound within which the genetic algorithm searches for the optimal cost. The bounds for the different variables are as follows:

- The number of PV panels was varied between 18 and 22 panels. HOMER software [48] was used to get a preliminary number of standard PV panels that meet the electrical load and that value is taken as the maximum number of modules plus or minus two modules.

- The number of PCM spheres required for each PV/T panel was varied between 50 and 100. The maximum number is associated with winter operation at low melting temperature of 30°C when PCM melt fraction would be very low while the minimum number of 50 is associated with the highest PCM melting temperature (37°C) during summer operation where the PCM temperature will reach more than 42°C.
- The melting temperature of the PCM varies between 30°C and 37°C. Smith et al. recommended melting points of 30°C to 35°C for the Mediterranean region when using PCM to enhance the photovoltaic energy output [37]. The range was expanded to 37°C in order to cover the summer and winter conditions.

A maximum population size equals to 20 times the number of variables with crossover fraction of 0.2, elite count of 2, and a function tolerance of 1×10^{-6} are set in the GA optimizer in order to arrive for the optimum values. The system costs C_{aux}, C_{PVT} and C_{PCM} are chosen to reflect the average prices in the Lebanese market where the cost of buying gas is $C_{aux}=0.05$ *$/kWh*, average cost of installing the PV/T panel $C_{PVT}=413$$ and the cost of 1 PCM sphere is $C_{PCM}=0.75$ *$*.

After solving for the design variables, the optimum values leading to the lowest system cost (PV/T panels and PCM) that minimizes the yearly cost of auxiliary heating energy while meeting the electrical needs over the whole system lifecycle, were found to be the following:

- The number of PV/T modules is 20 (4 kW at total area of 32 m^2 occupying 50% of the roof area)

- 72 PCM spheres each having a diameter of 7.5 cm and a mass of 311.5 grams are needed for each HP-PV/T-PCM panel. The PCM tank for each panel is built according to the required amount of PCM with an overall dimension of 92 cm × 47 cm × 8.5 cm (total volume of 37 liters) in order to contain the PCM spheres at the highest packing density while keeping the necessary space for the HP condensers and piping [49].
- The optimal melting temperature of the PCM is 33°C.

The HP-PV/T-PCM system's performance is simulated for the months of January, April, August, and October which are representative months of the four seasons of winter, spring, summer and fall, respectively. Figure 16 shows the hourly system power generation for the different representative months. It is observed that in the early morning and late afternoon, the power generation is less than the consumption because of the low solar radiation. In January, the power generation between 10:00 a.m. and 2:00 p.m. exceeds the office consumption, however over the whole day the generation is still less than the consumption. The power generation increases for months of April, August and October as the solar irradiance increases, and the excess is now enough to cover for the electricity deficit during low irradiance hours. August has the highest daily electricity production followed by April and October.

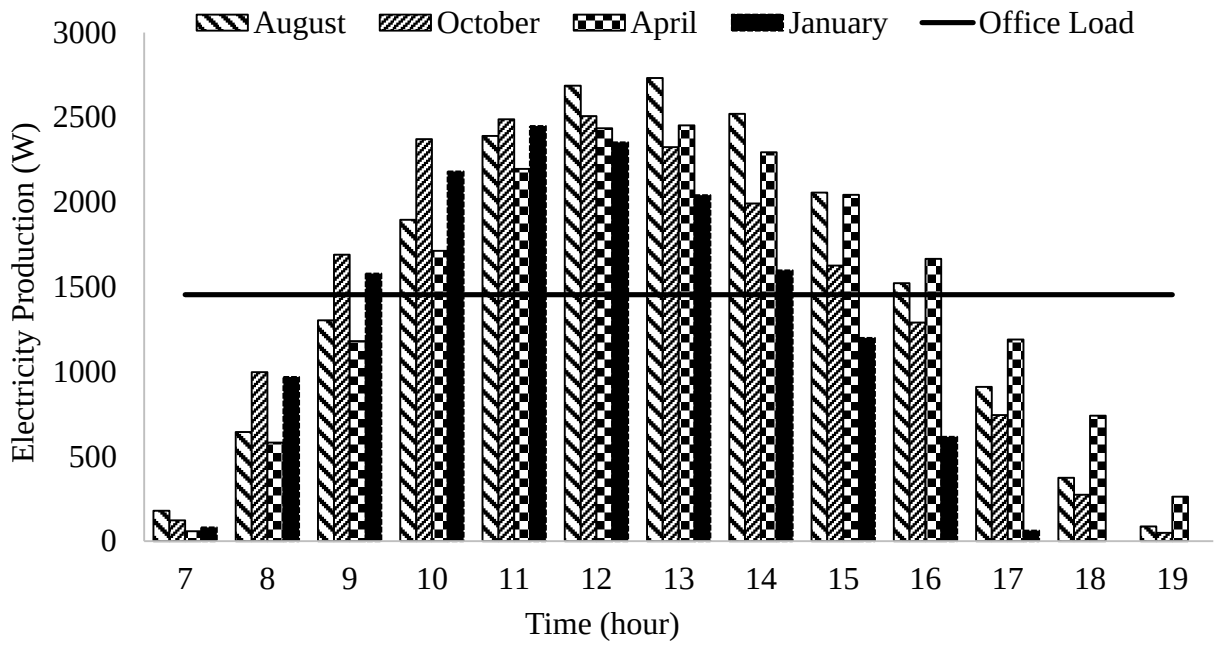

Figure 16: Plot of the hourly HP-PV/T-PCM power generation

It can be noticed from Table 4 that the electrical efficiency is at its best during the early morning and late afternoon, while during the rest of the day, the operating temperature of the cells increases leading to lower electrical efficiencies. January is characterized by the best efficiencies among the other months because of the low operating temperature of the PV panels during this month. During April, October and August, the increase in panel's temperature results in a drop in the electrical efficiency, while higher efficiencies are obtained in the morning and afternoon. August is characterized by the minimum efficiencies followed by October and April.

Table 4: Electrical and thermal efficiencies of the PV/T panels

Parameter	Hour											
	7-8	**8-9**	**9-10**	**10-11**	**11-12**	**12-13**	**13-14**	**14-15**	**15-16**	**16-17**	**17-18**	**18-19**
January												
η_{el}	12.23	11.85	11.48	11.11	10.68	10.78	10.81	10.94	11.4	11.72	0	0
η_{th}	0	0	0	7.8	8.43	8.1	6.13	0	0	0	0	0
η_{pvt}	32.18	31.18	30.21	48.44	36.53	32.1	34.58	28.79	30	30.84	0	0
April												
ηel	11.77	11.56	11.26	10.96	10.64	10.4	10.34	10.37	10.48	10.64	10.83	11.1
ηth	0	0	0	10.1	11.082	7.81	6.99	5.56	6.04	8	11.52	23.61
η_{pvt}	30.97	30.42	29.63	38.94	38.94	35.17	34.2	32.85	33.61	36	40.02	52.56
August												
ηel	11.64	11.47	11.19	10.89	10.56	10.3	10.22	10.23	10.4	10.54	10.74	10.96
ηth	0	0	0	13.66	19.08	14.69	13.3	12	13.93	29.26	31.02	35.3
η_{pvt}	30.63	30.18	29.45	42.38	46.87	41.8	40.19	38.92	41.3	57	59.28	64.14
October												
ηel	11.72	11.4	11.04	10.66	10.42	10.31	10.35	10.45	10.6	10.77	11.98	11.18
ηth	0	0	0	9.65	6.46	6.65	6.8	6.1	7.31	9.9	17.5	29.65
η_{pvt}	30.84	30	20.05	37.7	33.88	33.78	34.04	33.6	35.2	38.24	49.02	59.07

Table 5 presents the monthly electric consumption and generation for the months of study. January has the lowest total electrical consumption because of reduced pump operation hours compared to the other months. In January, the electricity production is less than the consumption, due to the low solar irradiance reaching the PV panels. During the months of higher solar irradiance, the electricity generation is found to be higher, and the electricity production exceeds the consumption. August has the highest electricity generation because of the highest amount of solar radiation reaching

the PV panels. The monthly electricity generation for the panels in January, April, August and October is 469.5 kWh, 584.9 kWh, 598.5 kWh and 573 kWh respectively. The yearly electricity production (6.67 MW) is found to exceed the yearly electricity consumption (6.39 MW) by 4.32%.

Table 5: Monthly Electric Energy Consumption and Production

Parameter	April	August	October	January
Electricity Consumption, kWh	544.45	544.45	544.45	542.47
HP-PV/T-PCM System Electricity Generation, kWh	584.9	598.5	573	469.45
Standard PV System Electricity Generation, kWh	557.9	566.2	548.77	457.9

The hourly heating energy supplied by the HP-PV/T panels to storage PCM-tank is shown in Fig.17 (a). The heating energy depends on the water temperature in the storage tank, the temperature of the PCM tanks, and the temperature and mass flow rate of the replacement water entering the storage tank according to the provided schedule (Table 3). It can be seen for all months that during the early hours of system operation there is no heat added by the HP-PV/T-PCM system to the water storage tank, where the PCM tanks' temperature is still lower than that of the storage tank. However, with the increase in the solar radiation, the PCM tanks' temperature increases and the system has enough energy to heat the water. For January, the heating energy increased to reach its maximum at 11 a.m. and then it decreased to reach zero after 1 p.m., where the water

temperature inside the office storage tank became higher than that in the PCM tanks. April, October and August have the same trend for the water heating energy, where this energy increased to reach its maximum at 12 noon due to the the high solar radiation from one side and increase in the water demand (Table 3). The heating decreased then to reach its minimum at 3 p.m. because of the reduced demand on hot water and decrease in the solar radiation. The heating energy continued to increase by the late afternoon as the demand for hot water increased, while the HP-PV/T-PCM system (which had stored energy in the PCMs) was still capable of providing useful heating energy to the office storage tank. Fig. 17(b) shows the hourly auxiliary heating requirements for the different representative months, where it is clear that the auxiliary heating was needed at the early hours of the system operation for all months and at the late afternoon for January.

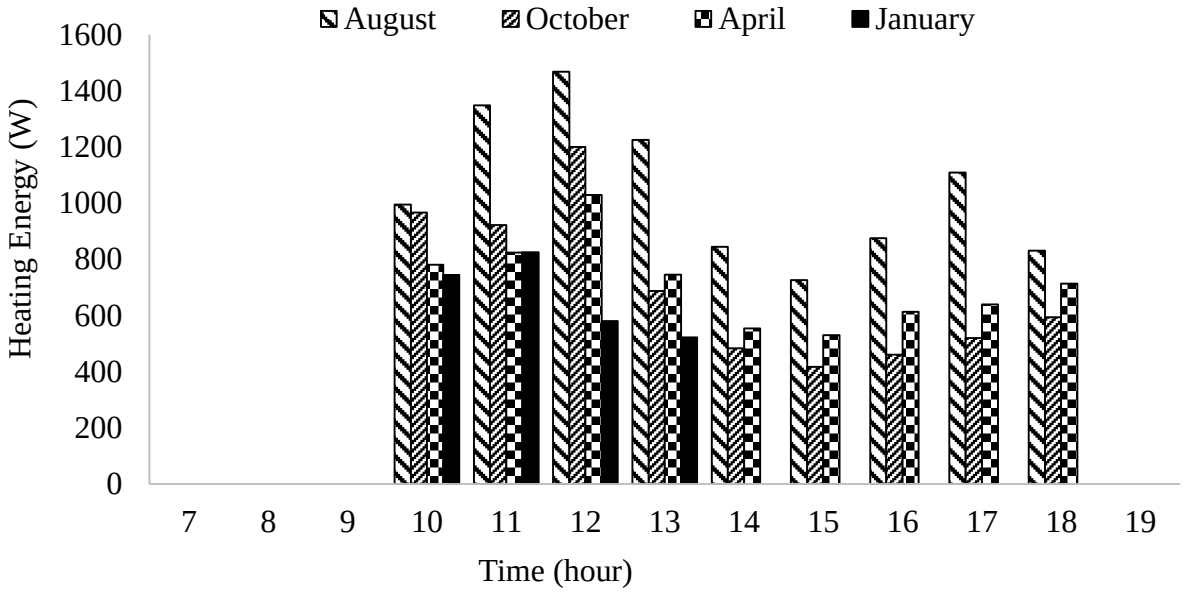

(a)

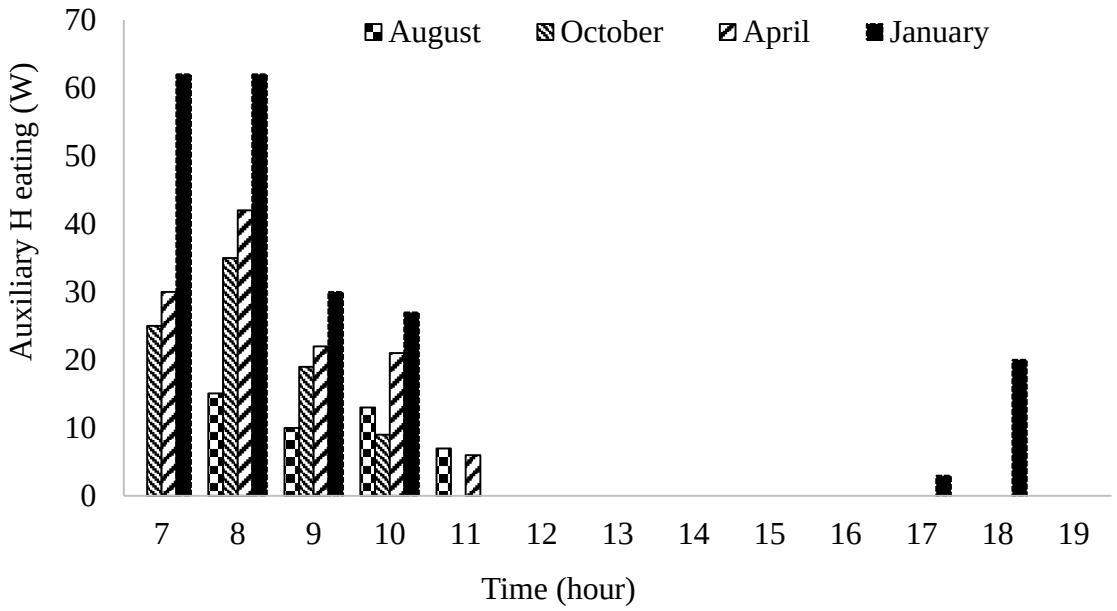

(b)

Figure 17: Plots of (a) the hourly HP-PV/T-PCM heating energy and (b) hourly auxiliary heat requirements for the representative months

According to Table 4, January shows the lowest thermal efficiencies and this is related to the low thermal heating energy provided by the HP-PV/T-PCM system due to the low amount of solar radiation and low ambient temperatures leading to high energy dissipation from the PCM tanks to the environment. The thermal efficiencies increased for months April, October and August with the increase in the solar radiation leading to higher temperatures of the PCM tanks and more amount useful heating thermal energy. The thermal efficiencies for these months continued to increase in the afternoon period and this is related to the decrease in the solar radiation, while the HP-PV/T-PCM system is still capable of supplying useful heating energy due to the presence of PCM. August has the highest thermal efficiencies among the other months. The average overall daily

efficiencies of January, April, August and October are 27.9%, 32.86%, 43.51%, and 34.61% respectively.

The monthly heating energy provided by the HP-PV/T-PCM system was highest for August (292 kWh) followed by April (199.224 kWh), October (193.62 kWh) and January (82.8 kWh), where it decreased with the decrease in the solar radiation and ambient conditions, with a total yearly of 2302.92 kWh. Accordingly, January was characterized by the highest amount of auxiliary heat needed (6.35 kWh/month), while August required the lowest amount (1.39 kWh/month) followed by April (2.7 kWh/month) and October (3.76 kWh/month). The total yearly auxiliary energy needed was 42.64 kWh.

When compared to the standard PV panels, it was observed that the efficiencies of the HP-PV/T-PCM panels improved by 4.53%, 6.62%, 6.26% and 8.7% at peak hours for months of January, April, October and August respectively. Moreover, the electricity generation of the HP-PV/T-PCM module is found higher than that of the standard PV panel for all months as shown in Table 4. The heat pipe cooling of the PV panels increased their yearly power output by 4.41 %, however the same number of panels (20 PV panels) in both cases is sufficient to cover the electrical needs.

A sensitivity analysis is performed on the system design with respect to the effect of deviation from optimal values of PCM number and melting temperature on system performance. It was found that decreasing the melting temperature of PCM by $1^{o}C$ caused an increase in the electrical efficiency of the PV/T panel by 0.177%, 0.204%, 0.212% and 0.25% and increased the monthly electrical production of the PV/T system by 0.005%, 0.06%, 0.08% and 0.13% for months of January, October, April and August respectively, with a 0.1% improvement in the total yearly electrical output.

However, decreasing the PCM melting temperature by 1°C resulted in an increase of the monthly auxiliary heat requirements by 0.743 kWh, 0.116 kWh, 0.067 kWh, and 0.03 kWh for months of January, October, April and August respectively with a yearly increase of 2.87 kWh. On the other hand, adding one PCM sphere in each HP-PV/T-PCM tank resulted in smaller increase of the PV/T panel electrical efficiency and insignificant change in auxiliary heat requirements. It is clear from this analysis that the optimal results are more sensitive to a one degree change in the melting temperature than adding one PCM sphere in each HP-PV/T-PCM tank.

The life cycle cost (LCC) assessment is performed for the proposed system and the payback period is calculated using the net present value (NPV). The LCC takes into consideration the initial investment cost for modifying the PV panels and the yearly operating cost over the lifespan of the system [50] taken as 25 years [37-39] (see eq. (19a and 19b)).The LCC and NPV are calculated as follows:

$$LCC = I + \sum_{i=1}^{N} \frac{C_i}{(1+a)^i} \tag{22}$$

Where I is the total modification cost of the system and C_i is the yearly cost for auxiliary heating (eq. 19b).

$$NPV_N = \sum_{i=1}^{N} \frac{R_i}{(1+a)^i} - LCC \tag{23}$$

where R_i is the revenue for year i. The project is considered profitable if $NPV_N > 0$

The cost of modifying the standard PV panel to a HP-PV/T-PCM panel is taken as $167/PV-T panel. The modification cost is chosen to reflect the prices in the Lebanese market, where it includes the cost of the base panel, heat pipes, PCMs and

different system materials. Having 20 panels resulted in an incremental cost of $3,380 including the piping connection and the system pump. On the other hand, the annual savings on heating water through the use of the HP-PV/T-PCM system were estimated as $276.3. Considering a discount rate of 1.5%, the payback period was found to be 13.7 years.

C. Conclusion

The feasibility of implementing a hybrid HP-PV/T system using phase change thermal storage has been evaluated. A theoretical model has been proposed to integrate the different system components. The model was validated by experiments. Good agreement was found between the model predictions and the experimental findings. The use of heat pipes and PCM was effective in providing a maximum reduction of 15^{o}C in the operating temperature of the PV panel at peak hour during the test day, followed by an increase of the electric power output and 9% improvement in the electrical efficiency, while providing hot water.

The HP-PV/T-PCM system was then applied to a typical office in Beirut City showing that finding optimal design is not a straightforward method and needs to take into consideration climate that influences the selection of the PCM melting point. A genetic algorithm optimization procedure was performed in order to decide for the best design of the system to meet the yearly electrical needs and minimize heating water energy for a typical office at the minimum number of PV panels and PCM quantity over the whole lifecycle (25 years). The yearly energy saving on heating water was estimated and the use of the PV/T system was found to be energy saving and cost effective with a payback period of 13.7 years.

BIBLIOGRAPHY

[1] Zondag HA. Flat-plate PV-Thermal collectors and systems: A review. Renewable and Sustainable Energy Reviews 2008;12(4): 891–959.

[2] Kumar R, Rosen MA. A critical review of photovoltaic-thermal solar collectors for air heating. Applied Energy 2011; 88(11): 3603–3614.

[3] Garg HP, Adhikari RS. Performance analysis of a hybrid photovoltaic/thermal (PV/T) collector with integrated CPC troughs. International Journal of Energy Research 1999; 23(15):1295-1304.

[4] Kumar R,. Rosen MA. Performance evaluation of a double pass PV/T solar air heater with and without fin. Applied Thermal Engineering 2011; 31(8):1402–1410.

[5] Tonui JK, Tripanagnostopoulos Y. Improved PV/T solar collectors with heat extraction by forced or natural air circulation. Renewable Energy 2007; 32(4):623-637.

[6] Odeh S, Behnia M. Improving Photovoltaic Module Efficiency Using Water Cooling. Heat Transfer Engineerin 2009; 30(6):499–505.

[7] Kalogirou SA. Use of TRNSYS for modelling and simulation of a hybrid pv–thermal solar system for Cyprus. Renewable Energy 2001; 23(2):247–260.

[8] Krauter S. Increased electrical yield via water flow over the front of photovoltaic panels. Solar Energy Materials and Solar Cells 2004; 82(1-2):131–137.

[9] Abdolzadeh M, Ameri M. Improving the effectiveness of a photovoltaic water pumping system by spraying water over the front of photovoltaic cells. Renewable Energy 2009; 34(1): 91–96.

[10] Wilson E. Theoretical and operational thermal performance of a ‘wet’ crystalline silicon PV module under Jamaican conditions. Renewable Energy 2009; 34(6): 1655–1660.

[11] Wu SY, Zhang QL, Xiao L, Guo FH. A heat pipe photovoltaic/thermal (PV/T) hybrid system and its performance evaluation. Energy and Buildings 2011; 43(12): 3558–3567.

[12] Gang P, Huide F, Tao Z, Jie J. A numerical and experimental study on a heat pipe PV/T system. Solar Energy 2011; 85(5): 911–921.

[13] Mathioulakis E, Belessiotis V. A New Heat-pipe Type Solar Domestic Hot Water System. Solar Energy 2002; 72(1): 13-20.

[14] Azad E. Assessment of three types of heat pipe solar collectors. Renewable and Sustainable Energy Reviews 2012; 16(5): 2833-2838.

[15] Hammad M. Experimental Study of the performance of a solar collector cooled by heat pipes. Energy Conversion and Management 1995; 36(3): 197–203.

[16] Ghaddar N, Nasr Y. Experimental Study of a Refrigerant Charged Solar Collector. International Journal of Energy Research 1998; 22(7): 625-638.

[17] Huang BJ, Lin TH, Hung WC, Sun FS. Performance evaluation of solar photovoltaic/thermal systems. Solar Energy 2001; 70(5): 443–448.

[18] Abhat A. Low-temperature latent heat thermal storage: heat storage materials. Solar Energy 1983; 30(4) : 313–332.

[19] Sharma A, Tyagi VV, Chen CR, Buddhi D. Review on thermal energy storage with phase change materials and applications. Renewable and Sustainable Energy Reviews 2009; 13(2): 318–345.

[20] Prakash J, Garg HP, Datta G. A solar water heater with a built-in latent heat storage. Energy Conversion and Management 1985; 25(1): 51–56.

[21] Cabeza LF, Ibáñez M, Solé C, Roca J, Nogués M. Experimentation with a water tank including a PCM module. Solar Energy Materials and Solar Cells 2006; 90(9): 1273–1282.

[22] Cabeza LF, Ibáñez M, Solé C, Roca J, Nogués M. Modelization of a water tank including a PCM module. Applied Thermal Engineering 2006; 26(11): 1328–1333.

[23] Duffie JA, Beckman WA. Solar Engineering of Thermal Processes, 3rd ed. USA: John Wiley & Sons. 2006.

[24] Oosthuizen PH. Experimental Study of Free Convective Heat Transfer From Inclined Cylinders. Journal of Heat Transfer 1976; 98(4): 672–674.

[25] Azad E. Theoretical and experimental investigation of heat pipe solar collector. Experimental Thermal and Fluid Science 2008; 32(8): 1666-1672.

[26] McAdams, WH. Heat Transmission, 3rd ed., New York: McGraw-Hill, 1954.

[27] Hussein HMS, Mohamad MA, El-Asfouri AS. Optimization of a wickless heat pipe flat plate solar collector. Energy Conversion and Management 1999; 40(18): 1949-1961.

[28] Incropera FP, Dewitt DP, TL Bergman, Lavine AS. Fundamentals of heat and mass transfer, 6th ed. USA: John Wiley & Sons. 2007.

[29] Yang L, Zhang XS. Performance of a new packed bed using stratified phase change capsules. International Journal of Low-Carbon Technologies 2012; 7(3): 208-214.

[30] Torres Ledesma J, Lapka P, Domanski R, Casares FS. Numerical simulation of the solar thermal energy storage system for domestic hot water supply located in south Spain. Thermal Science 2013; 17(2): 431-442.

[31] Mozumder AK, Akon AF, Chowdhury MSH, Banik SC. Performance of heat pipe for different working fluids and fill ratios. Journal of Mechanical Engineering 2010; 41(2): 96-102.

[32] Mitchell M. An Introduction to Genetic Algorithm. Cambridge: The MIT Press 1997.

[33] Jong K. Learning with Genetic Algorithms: An Overview. Machine Learning 1988; 3(2-3): 121-138.

[34] Ali S, Kim DH. Optimized Power Control Methodology Using Genetic Algorithm. Wireless Personal Communications 2015; 83(1): 493-505.

[35] Amin NAM, Mohamad A, Abdul Majid MS, Afendi M, Bruno F, Belusko M. Experimental Investigation of PCM Spheres in Thermal Energy Storage System. Applied Mechanics and Materials 2013; 367: 228-233.

[36] Campos Celador A, Odriozola M, Sala JM. Implications of the modelling of stratified hot water storage tanks in the simulation of CHP plants. Energy Conversion and Management 2011; 52(8-9): 3018-3026.

[37] Smith CJ, Forster PM, Crook R. Global analysis of photovoltaic energy output enhanced by phase change material cooling. Applied Energy 2014; 126: 21-28.

[38] Kannan R, Leong KC, Osman R, Ho HK, Tso CP. Life cycle assessment study of solar PV systems: An example of a 2.7 kW_p distributed solar PV system in Singapore. Solar Energy 2006; 80(5): 555-563.

[39] www.teappcm.com. Accessed on June 16, 2014.

[40] Swapnil D, Tiwari GN. Analysis of PV/T flat plate water collectors connected in series. Solar Energy 2009; 83(9): 1485-1498

[41] ASHRAE Standard 90.1. Energy Standard for Buildings Except Low-Rise Residential Buildings. 2007.

[42] Ulseth R, Alonso MJ, Haugerud LP. Measured load profiles for domestic hot water in buildings with heat supply from district heating. The 14th International Symposium on District Heating and Cooling. Stockholm, Sweden 2014.

[43] http://www.engineeringtoolbox.com/hot-water-consumption-person-d_91.html

[44] U.S Food and Drug Administration. 2005 Food Code. U.S Department of Health and Human Services.

[45] Garg HP, Agarwal RK. Some aspects of a PV/T collector/forced circulation flat plate solar water heater with solar cells. Energy Conversion and Management 1995; 36(2):87-99.

[46] Ghaddar N, Bsat A. Energy conservation of residential buildings in Beirut. International Journal of Energy Research 1998; 32(2): 523–46.

[47] ASHRAE Handbook: Fundamentals. American Society of Heating, Refrigeration and Air-Conditioning Engineers, Inc. 2005.

[48] HOMER Software, Laboratory National Renewable Energy. Colorado, USA, 2014.

[49] Patil RM, Ladekar C. Experimental Investigation for Enhancement of Latent Heat Storage using Heat pipes in Comparison with Copper Pipes. International Refereed Journal of Engineering and Science 2014; 3(9): 44-52.

[50] Cryder J, Lally M. Life Cycle Cost Analysis. School and college (Cleveland, Ohio) 2008; 47(11): 30.